AD-A114 661 PRINCETON UNIV NJ DEPT OF CHEMICAL ENGINEERING F/G 4/1
CHEMICAL REACTIONS AND MOLECULAR AGGREGATION IN CRYOGENIC WHOLE--ETC(U)
JAN 82 J M CALO, R J FEZZA, G F RYAN F19628-80-C-0066
UNCLASSIFIED AFGL-TR-82-0061 NL

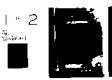

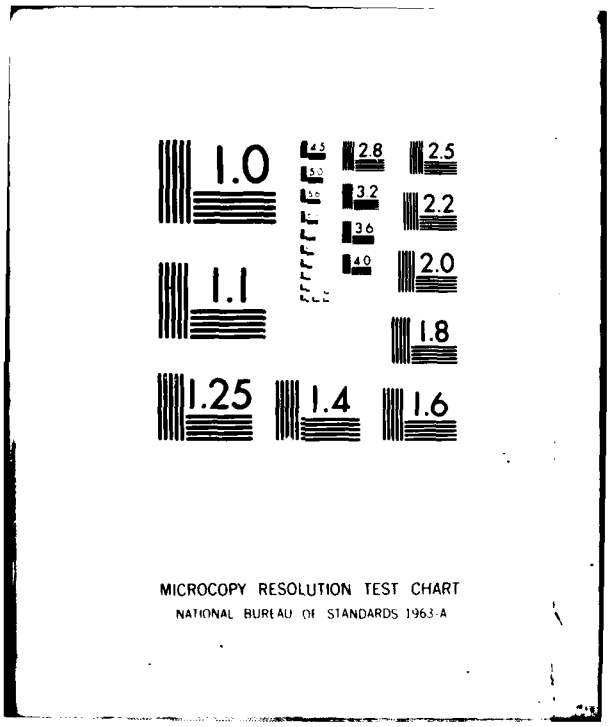
1.0
1.1
1.25
1.4
1.6
1.8
2.0
2.2
2.5
2.8
3.2
3.6
4.0
4.5
5.0
5.6
MICROCOPY RESOLUTION TEST CHART
NATIONAL BUREAU OF STANDARDS 1963-A

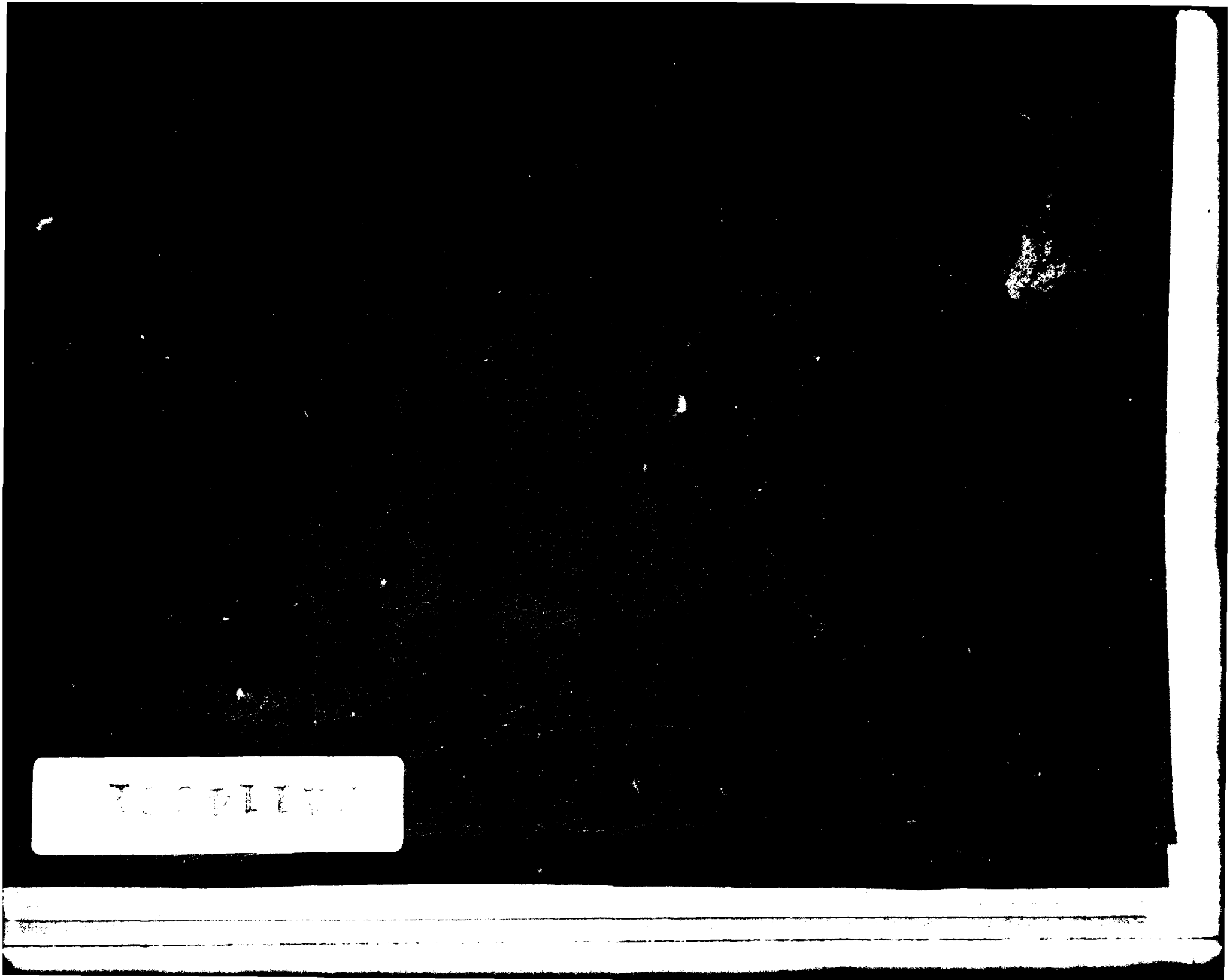

Unclassified

SECURITY CLASSIFICATION OF THIS PAGE (When Data Entered)

REPORT DOCUMENTATION PAGE	READ INSTRUCTIONS BEFORE COMPLETING FORM
1. REPORT NUMBER: AFGL-TR-82-0061	2. GOVT ACCESSION NO.: AD-A114661
3. RECIPIENT'S CATALOG NUMBER	
4. TITLE (and Subtitle): CHEMICAL REACTIONS AND MOLECULAR AGGREGATION IN CRYOGENIC WHOLE AIR SAMPLE MATRICES	5. TYPE OF REPORT & PERIOD COVERED: Final Report for Period 1 March 1980-30 Sept.81
	6. PERFORMING ORG. REPORT NUMBER
7. AUTHOR(s): J. M. Calo, R. J. Fezza, G. F. Ryan	8. CONTRACT OR GRANT NUMBER(s): F19628-80-C-0066
9. PERFORMING ORGANIZATION NAME AND ADDRESS: Department of Chemical Engineering Princeton University Princeton, New Jersey 08544	10. PROGRAM ELEMENT, PROJECT, TASK AREA & WORK UNIT NUMBERS: 62101F,668703AL
11. CONTROLLING OFFICE NAME AND ADDRESS: Air Force Geophysics Laboratory Hanscom AFB, Massachusetts 01731 Monitor/Charles C. Gallagher/LKD	12. REPORT DATE: January 1982 13. NUMBER OF PAGES: 110
14. MONITORING AGENCY NAME & ADDRESS(if different from Controlling Office)	15. SECURITY CLASS. (of this report): UNCLAS 15a. DECLASSIFICATION/DOWNGRADING SCHEDULE
16. DISTRIBUTION STATEMENT (of this Report): "Approved for public release; distribution unlimited."	
17. DISTRIBUTION STATEMENT (of the abstract entered in Block 20, if different from Report)	
18. SUPPLEMENTARY NOTES	
19. KEY WORDS (Continue on reverse side if necessary and identify by block number): Cryogenic sampling of atmospheric gases; stratospheric species; chemical reactions in cryofrosts	

20. ABSTRACT (Continue on reverse side if necessary and identify by block number)

Chemical reactions and molecular aggregation phenomena in cryogenic condensates associated with in-situ cryogenic whole air sampling of stratospheric species are examined. Results for two types of studies are reported.

In the first, type, the gas phase composition resulting from thermal desorption of pure and mixed condensates collected on the

DD FORM 1 JAN 73 1473 EDITION OF 1 NOV 65 IS OBSOLETE
S/N 0102-014-6601 |

Unclassified

SECURITY CLASSIFICATION OF THIS PAGE (When Data Entered)

cold end of a mechanical, helium-cycle, cryogenic refrigerator is determined with mass spectrometry and NO_x chemiluminescence (when possible). This technique was applied to studies of the reactions of nitric oxide and ozone upon thermal desorption. The most salient results were: (1) disproportionation of nitric oxide to nitrogen dioxide and nitrogen during desorption of pure nitric oxide condensate at levels exceeding 50%; (2) significant recombination of ozone upon flash desorption; and (3) oxidation of nitric oxide to nitrogen dioxide by ozone upon desorption of nitric oxide/ozone condensates.

The second technique involves the direct observation of species behavior in the cryogenic condensate upon warming with infrared spectrophotometry. Essentially, an IR cell was constructed from a PVC vacuum shroud (fitted with CdTe windows to allow the IR beam to enter and exit) enclosing the cold end of the cryogenic refrigerator. A CdTe disk in a copper holder screwed into the cold end serves as the cryosurface for sample collection and allows IR transmission through the sample. The entire system is situated in the beam path of an IR spectrophotometer. Preliminary operational data and spectra for stratospheric species are reported.

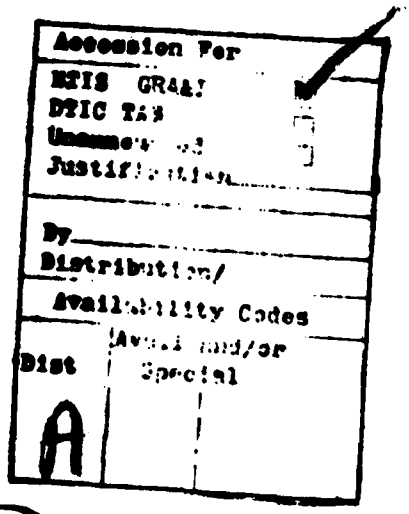

SUMMARY

This final report summarizes the work performed and the accomplishments during the first nineteen months of a three-year project concerned with chemical reaction and molecular aggregation phenomena in cryogenic condensates relevant to in-situ, cryogenic whole air sampling of the stratosphere. This project was initiated and funded under AFGL Contract No. F19628-80-C-0066 at Princeton University on 1 March 1980. However, the move of the principal investigator from Princeton University to Brown University necessitated termination of the contract at Princeton on 30 September 1981. Work on the original project is being continued at Brown University under a new successor contract (AFGL F19628-81-C-0157).

Results from two distinct types of studies are reported. One focusses on the measurement of the gas phase composition resulting from thermal desorption of condensate collected on the cold end of a mechanical helium-cycle, cryogenic refrigerator, with mass spectrometry and NO_x chemiluminescence (when possible). This approach was applied to both temperature programmed and flash desorption studies of NO_x-O_x cryogenic condensates. Results include: (1) A surprisingly persistent self-disproportionation of NO to NO_2 (viz., $4NO \rightarrow 2NO_2 + N_2$) upon desorption of both pure and NO-containing condensates at conversion levels exceeding 50%. A self-catalytic mechanism is hypothesized. (2) Ozone was found to recombine upon desorption, exhibiting

a threshold effect related to the quantity of deposit. A marked aging effect of the gold-flashed, stainless steel cryosurface was noted, with catalytic activity towards ozone recombination increasing steadily with time, possibly due to metal oxide formation on small areas of exposed steel. (3) A significant level of oxidation of NO to NO_2 by ozone was also observed over and above that produced by NO disproportionation.

The second type of study involves the direct observation of species behavior in the cryogenic condensate upon warming with infrared spectrophotometry. Essentially, an IR cell was constructed from a PVC vacuum shroud (fitted with CdTe windows to allow the IR beam to enter and exit) enclosing the cold end of the cryogenic refrigerator. A CdTe disk in a copper holder screwed into the cold end serves as the cryosurface for sample collection and allows IR transmission through the sample. The entire system is situated in the beam path of an IR spectrophotometer. Preliminary operational data and spectra for stratospheric species are reported.

Table of Contents

List of Figures

List of Figures (continued)

List of Tables

1. INTRODUCTION

In an early unpublished research proposal examining the prospects of cryogenic sampling of the atmosphere, Snelson (1972) exploited the advantage of the naturally high dilution of reactive atmospheric species in an air sample matrix. He noted that a cryofrost of atmospheric species would have nitrogen and oxygen as the primary matrix material with trace species "locked" into the matrix structure at parts per million, and lower, concentrations. Thus these species would be matrix-isolated, with N_2 and O_2 as nearest neighbors, and any possible reactions would be severely limited by the low temperature and extremely low diffusion rates. Snelson argued that many species could be studied directly in the solid phase by electron paramagnetic resonance (EPR) spectroscopy (e.g., O_3, CHO, CH_2, CH_3, and other radicals), or after gamma or ultraviolet irradiation (e.g., CO_2, CO, CH_4). Snelson realized, however, that many other species would require alternate analytical techniques, such as gas chromatography (GC) e.g., O_2, H_2O, N_2O, SO_2), which would entail thermal desorption and possibly fractional distillation of the sample.

The inherent advantages of matrix isolation would be lost with such analytical techniques, and the chemical composition of the sample could be altered. Due to the extremely low concentrations of free radical species in the frost, however, Snelson (1972) argued that reactions would not appreciably alter the other constituents.

In the cryogenic whole air sampling project of the

Stratospheric Environment Program of the Air Force Geophysics Laboratory, as reported by Gallagher and Pieri (1976) and Gallagher, Pieri, and Goldan (1977), all the post-sampling analytical procedures require the regeneration of the cryofrost, and thus loss of matrix isolation. Here we examine the effects of these manipulations on possibly reactive species, in particular, the oxides of nitrogen (NO_x) and ozone, which are of primary stratospheric importance.

Many references in the extant literature support the possibility of reactions between what Snelson (1972) considered to be "stable" molecular species. Smith and Guillory (1977) reported the thermal oxidation of dimerized NO by O_2 in the solid phase in the 13K to 29K temperature range. Lucas and Pimentel (1979) cite the thermal oxidation of NO with O_3 while matrix isolated within N_2 in typical $NO/O_3/N_2$ ratios of 1/30/250, between 11K and 20K in the solid phase. Explosion hazards involved with the handling of concentrated, condensed ozone are also well known. For example, Arin and Warneck (1972) noted the rapid reaction of O_3 with CO at low pressure and room temperature, Deitz and Bitner (1973) encountered an explosive reaction while adsorbing O_3 onto charcoal, and Jenkins (1959) reported spontaneous explosion of liquid O_3 at 90K, in which a catalytic impurity was suspected. Thus thermal regeneration of cryofrosts involving these species and others, including radicals, may also be expected to exhibit similar reactions which would then serve to alter or mask "true" relative ambient stratospheric composition.

As a result of previous experience with cryofrosts composed of stratospheric species (Calo et. al., 1981), the capability of determining how gaseous species adsorb on cryogenic surfaces and how multicomponent cryofrosts desorb upon warming was developed. In the current work, we report the results of studies directed at understanding reactions in the cryofrost indirectly using mass spectrometric and NO_x-ozone chemiluminescence techniques of the gas phase upon thermal or flash desorption of condensed cryofrosts. We also report progress on applying infrared spectrophotometry to the direct observation of species behavior in the cryofrost while in residence. This work is novel in that much has been published concerning matrix isolation at low temperatures, while relatively little is known about the processes which occur upon heating the matrix to desorption; e.g., the effects of catalysis, morphology, and contaminants.

REFERENCES

Arin, L. M. and P. Warneck, J. Phys. Chem. 76, 1514 (1972).

Calo, J. M., R. J. Fezza, and E. J. Dineen, "Gas-Surface Interactions in Cryogenic Whole Air Sampling", AFGL-TR-81-0162, Air Force Geophysics Laboratory, Hanscom AFB, MA, May 1981.

Gallagher, C. C., Pieri, R. V., AFGL-TR-76-0161, July, 1976.

Gallagher, C. C., Pieri, R. V., Goldan, P. D., J. Atm. Sci. 34, 1481-2, 1977.

Deitz, V. R. and J. L. Bitner, Carbon 11, 393 (1973).

Jenkins, A. C., Ozone Chemistry and Technology, Adv. Chem. Series, ACS, Washington, D. C., 1959, pp. 13-21.

Lucas, D. and G. C. Pimentel, J. Phys. Chem. 83, 2311 (1979).

Smith, G. R. and Guillory, W. A., Int. J. Chem. Kin. IX, 953 (1977).

Snelson, A., "The Chemical Composition of The Atmosphere at 40,000-65,000 Feet Using a Modified Matrix Isolation Technique", Project Suggestion #IITRI-72-107CX, IIT Research Institute, Ill., 1972.

2. EXPERIMENTAL

Essentially two different experimental systems were used in the studies reported here. The first apparatus was essentially the same as used in our previous work (Calo et.al., 1981) and employs mass spectrometric and chemiluminescence analysis of the resultant gas phase upon thermal desorption of cryofrosts. The other, more recent apparatus has been designed to allow transmission infrared spectrophotometry of cryofrost samples. These two systems are described below in turn.

2.1 Gas Phase Thermal Desorption System

The apparatus developed for these studies is schematized in Figure 2-1. The primary functions of the experimental system are to allow controlled deposition and subsequent desorption of the various gases and vapors of interest onto and from a cryogenic surface while monitoring gas phase compositions with appropriate analytical techniques.

The apparatus consists of a closed cycle, cryogenic refrigerator (Air Products, Displex CS202, closed-cycle, helium refrigerator) upon which can be mounted a disk of the cryosurface material under consideration (e.g., electropolished, gold-flashed, or hexamethyldisilazane-coated 304 stainless steel). The cryosurface temperature was monitored with a silicon diode sensor and a digital thermometer-controller (Lake Shore Cryotronics, DRC-7C) capable of temperature measurements in the 1-400K range with an accuracy of $\pm$ 1K. The refrigerator is capable of maintaining the cryosurface at 10K

under conditions of zero heat load in vacuo. In practice, however, a lower temperature limit of 14K was routinely achieved, primarily due to the absence of a radiation shield.

The cryosurface disk was juxtaposed by a quadrupole mass spectrometer positioned with its axis parallel to the cryosurface normal, centered, and located such that the extreme end of the electron impact ionizer head was 0.94 inches away. Both the refrigerator and the mass spectrometer were maintained in a conventional, liquid nitrogen-trapped, diffusion pumped vacuum chamber. The chamber was also equipped with ribbed stainless steel coils which could be cooled with liquid nitrogen in order to provide additional cryopumping for species condensable at these conditions, if so desired.

Gases were introduced via a Granville-Phillips variable leak valve. The feed tubulation terminated in a 1 mm I.D. tube positioned 5 mm from the cryosurface so that the centerline of the resultant molecular beam was normal to the cryosurface and aligned with its center. The flow from this tube was determined to be effusive. Most of the sample gases were introduced directly from gas cylinders, with the exception of ozone which was generated in pure oxygen in a high voltage DC discharge laboratory ozonator to an upper limit of 2.25% ozone in oxygen.

2.1-1. Pumping Speed Calibrations

The conductance-limited pumping speed of the vacuum system was determined without cryopumping, by two separate

methods. The first is a technique proposed by Dushman (1949), in which the vacuum chamber is raised to an elevated pressure by the addition of a leak stream, which is then instantaneously shut off. The pressure of the chamber is then followed as it returns to its base pressure. Application of continuity, i.e.,

$$\overset{o}{V}/V_s = -dP/Pdt \qquad (2.1\text{-}1)$$

where

$\overset{o}{V}$ = system pumping speed (ℓ/s)

V_s = system volume (ℓ)

P = system pressure (torr)

t = time (s)

yields the instantaneous pumping speed of the system. Table (2.1) presents data for three such experiments, performed on three separate occasions. Since conductance-limited pumping should occur at constant speed, and noting that V_s = 8.9 liters, averaging the V/V_s values and multiplying by V_s, yields V = 17.0 ℓ/s with a standard deviation of $\pm$1.15 ℓ/s.

The second technique employed a calibrated glass nozzle positioned in a feedthrough to the vacuum chamber, the foreline pressure of which was monitored with a Baratron diaphragm-type pressure transducer. The nozzle orifice was first calibrated on a roughing pump line with one side of the nozzle at atmospheric pressure and the other under vacuum.

Since these conditions assured sonic flow (Liepmann and Roshke, 1957):

$$\overset{o}{V} = \left(1 + \frac{1}{2} M^2 (\gamma-1)\right)^{-\left(\frac{1}{\gamma-1}\right)} \left[M\left(\frac{R\gamma T_o}{MW}\right)^{1/2}\right]\left(1 + M^2 \frac{\gamma-1}{2}\right)^{-1/2} \qquad (2.1\text{-}2)$$

where

M = Mach number of flow at nozzle throat = 1

γ = C_p/C_v for species of interest

R = gas constant

MW = molecular weight

A = cross sectional area of the orifice

In this manner it was found that the nozzle had a diameter of 0.01245 cm. This nozzle was then installed, as described, on the high vacuum chamber. Systematic variation of the pressure applied to the nozzle yielded the data contained in Table (2.2). The pumping speed of the chamber was then calculated employing both the sonic flow equation (2.1-2) ($\overset{o}{V}_{sonic}$) and that for effusive flow ($\overset{o}{V}_{effusive}$), i.e.,

$$N = \frac{\pi}{4} d^2 n \frac{1}{4} \left(\frac{8kT}{\pi MW}\right)^{1/2} \qquad (2.1\text{-}3)$$

where

N = molecular flow (molecules/s)

n = upstream number density

d = orifice diameter

as given in Davidson (1962). This approach was necessitated by the fact that the ratio of the mean free path of the gas to the diameter of the nozzle (L_a/D, Table (2.1-2)) was close to one, which raises the possibility that the flow might not be sonic. Figure (2-2) presents the results of the pumping

speeds determined using both assumptions versus L_a/D for the nozzle. Note that for $L_a/D>0.3$, the pumping speed remains relatively constant at approximately 17.6 ℓ/s, whereas below this value, it drops off sharply. This behavior is interpreted as indicating that the nozzle flow is effusive for $L_a/D>0.3$. The calculated sonic pumping speed approaches the effusive pumping speed at values for $L_a/D<0.3$. Thus, the conduction-limited pumping speed of the system was assumed to be 17.6 ℓ/s, which agrees quite well with the value determined with the alternate technique.

2.1-2. NO_x Chemiluminescence Analyzer Modification, Operation, and Calibration.

It has been observed experimentally that NO_2 and O_3 do not exhibit mass spectrometer parent peaks at m/e of 46 and 48, respectively. Their cracking pattern includes fragment peaks located at m/e ratios of other species of interest; e.g., NO_2 exhibits peaks at 30, as for NO; 16 and 14 as for NO; while O_3 has peaks at 16 and 32, as does O_2. Therefore, it is not possible to use the mass spectrometer to distinguish NO_2 from NO, and O_3 from O_2. All attempts at altering the fragmentation patterns of NO_2 and O_3 to obtain a parent peak were unsuccessful. Therefore, the Thermoelectron Model 10AR NO_x chemiluminescence analyzer, schematized in Figure 2-3, was employed.

The chemiluminescence analyzer allows independent analysis for NO and NO_2 and relies on the reaction between ozone and nitric oxide:

$$NO + O_3 \xrightarrow{(\alpha)} NO_2 + O_2$$

which produces a certain fraction of electronically excited NO_2, $^{(1-\alpha)}$,

$$NO + O_3 \xrightarrow{(1-\alpha)} NO_2^* + O_2$$

that spontaneously deactivates to the ground state giving off a photon in the 600-2500 nm wavelength range:

$$NO_2^* \longrightarrow NO_2 + h\nu$$

Detection of these photons is used to determine the concentration of NO in the sample gas. In order to measure the concentration of NO_2 in the sample, the gas is first passed through a stainless steel reactor coil maintained at 650°C which quantitatively thermally reduces NO_2 to NO.

In addition to measuring NO/NO_x the chemiluminescence analyzer was modified by adding a manifold with two valved feed ports on the oxygen-ozone feed line to the reactor which enabled bypassing the internal ozone generator, thereby also allowing the use of either internally generated ozone or an ozone-containing feed stream. A standard 5% NO in N_2 mixture, in lieu of the conventional sample, could then be used to measure the ozone content of a feed stream. In modifying the chemiluminescence analyzer for ozone titration; several flow rates and concentrations were changed. Thus, in order to insure accuracy, the analyzer was calibrated against a standard ozone analytical technique as follows. To insure reproducibility of ozone concentrations, the Welsbach ozone generator was always set at an oxygen feed rate of 2 SLPM (standard liters per

minute) at 8 psig, and only the primary voltage of the ozonator was changed to vary the ozone concentration. A schematic of the calibration apparatus is presented in Figure (2-4). The materials employed were limited to glass, stainless steel, teflon, and tygon, as recommended by Welsbach (1977). As shown in Figure (2-4), the bulk of the ozonated oxygen was fed to a scrubber filled with a potassium iodide solution, which chemically destroys ozone. Upstream of the scrubber, two bleed lines allowed the ozonated oxygen to be fed either directly to the chemiluminescence analyzer, or to the ozone titration apparatus.

The bleed stream to the chemiluminescence analyzer passes through the gas sampling and feed apparatus for the main vacuum chamber (i.e., the leak valves, etc.) employed in the actual experiments. Thus any ozone loss due to adsorption and recombination in the equipment feed system, however slight, is essentially nulled out in the calibration process. The flow rate into the chemiluminescence analyzer was maintained constant and reproducible by setting the pressure just upstream of the 9 inch length of 0.02 inch I.D. capillary tubing (Figure 2-1) to 19.9 in. Hg, with the sampling system leak valve. Gas flows directly from the capillary to the reactor within the chemiluminescent analyzer, where a second feed containing 5% NO in N_2 (Matheson, unanalyzed) is introduced, and the resultant luminescence is detected by a photomultiplier tube, the signal from which is amplified and read out on a

panel meter. Since concentrations and flowrates of the two streams were altered, the analyzer panel meter did not read the concentration of O_3 directly, thereby necessitating recalibration.

The second bleed stream shown in Figure (2-4) leads to a wet calibration apparatus, as recommended by Welsbach (1977). The gas flow, regulated by a stainless steel valve, is fed through a gas bubbler (medium porosity) containing 400 ml of 2% potassium iodide solution at approximately 0.3 ℓ/min. In the bubbler, the reaction:

$$O_3 + 2I^- + H_2O \longrightarrow O_2 + I_2 + 2OH^-$$

takes place. The gas, now stripped of ozone, passes through a pressure gauge and then through a wet test meter, where its volume is recorded as a function of time. The iodine solution produced in the bubbler is then removed and acidified with 10 ml of 1M sulfuric acid and titrated with either 0.1 or 0.01 N sodium thiosulfate solution, depending on the suspected concentration of the iodine solution. Starch solution is used as an indicator, and is added when the bright yellow color of the solution begins to fade.

The information derived from this wet titration, along with the sample gas volumetric flow data (corrected for saturation with water vapor), allows the determination of ozone concentrations in the sample gas stream. Welsbach (1977) contends that this wet titration technique is accurate to $\pm$ 1% of the amount of O_3 in the sample stream in concentrations down to approximately 28 ppm.

Using the wet titration apparatus, the ozone concentration in the product stream was also calibrated against the primary voltage of the Welsbach ozonator. It was found that an ozone concentration of 2.24% $\pm$ 0.1% could be delivered reproducibly. Since high concentrations of ozone in the feed gas were desired, this particular concentration was employed in the experiments discussed below.

The actual calibration curve of wet titration results versus chemiluminescence analyzer readings is given in Figure 2-5. The entire calibration range is fit reasonably well by a third order polynomial with least squares coefficients; viz.,

$$C = 3.887 \times 10^{-2} + 0.130I - 2.322 \times 10^{-6} I^2 + 1.2208 \times 10^{-9} I^3,$$

where C is the titrated ozone concentration, in ppm, and I is the chemiluminescence analyzer meter reading, also in ppm. From this calibration it can be seen that the chemiluminescence analyzer, when operated in this fashion, is approximately an order of magnitude more sensitive than when operated in its normal mode; i.e., the normal resolution of $\pm$ 0.1 ppm for the lowest range becomes $\pm$ 0.01 ppm for ozone. This increased sensitivity was useful in the experimental work.

Two different types of experiments were conducted with this system. One is temperature programmed desorption (TPD). In TPD experiments, the cryosurface temperature is allowed to increase by conduction of heat along the refrigerator stem.

This technique allows a slow, reproducible temperature increase with time. Mass spectrometry, rather than chemiluminescence, is used to monitor the species of interest. Care must be taken, however, since some parent peaks of low level vacuum chamber contaminants; e.g., the N_2 parent peak at m/e 28 is also the parent peak of CO, a common vacuum chamber contaminant. In order to minimize these problems, background desorption spectra are subtracted from the desorption spectrum of the species of interest. Care was taken to insure that the absolute sample amount did not cause the vacuum system pressure to exceed its operating limits upon thermal desorption. The typical total deposit amount for a TPD experiment was approximately 10^{-5} g mol.

In order to employ the chemiluminescence analyzer to detect NO, NO_2, and O_3 desorbed in the experimental apparatus, a gas sample at or near atmospheric pressure must be available. In order to meet this requirement, a second type of experiment was devised, which is referred to here as flash desorption (FD). For FD, a more massive cryofrost sample, typically 10^{-3} g mol, is deposited on the cryosurface. Then, instead of slow desorption and <u>in situ</u> analysis, as in TPD, the experimental vacuum chamber is sealed off from the pumping system and filled with N_2 to approximately 5 psig through the nozzle system. The final system pressure is measured with a Bourdon gauge, which, together with the chamber volume, allows a quantitative determination of desorbed gas concentrations.

This technique has the advantage of an increased desorption rate as compared to TPD, and rapid dilution of components in the gas phase, which limits gas phase reactions, thereby restricting any potential reactive effects to those occurring in the solid state or during the transition to the gaseous state. Figure (2-6) illustrates typical temperature versus time curves for both TPD and FD type experiments. Note that the employing FD, the cryosurface reaches approximately 183K in 4 minutes, while with TPD the surface would still be at 44K.

2.2 Infrared Spectrophotometry System

The apparatus developed for direct, in-situ observation of the behavior of species in the cryogenic condensate as a function of deposition rate, dilution, heat treatment (annealing) and temperature is shown in Figure (2-7).The primary function of this experimental system is to enable controlled deposition of various gases and vapors onto a temperature-controlled cryogenic surface which allows sufficient transmission of infrared radiation to obtain infrared spectrophotometric data.

The apparatus makes use of the same closed cycled cryogenic refrigerator employed in the system described previously (i.e., Air Products Displex CS202, closed-cycle, helium refrigerator) to cool the IR transmission window/cryosurface. In the current work, this window was a polycrystalline CdTe disk, 1 in. in diameter and 0.125 in. in thickness (~65% transmission, 4000-400 cm^{-1}). This window was clamped in the copper holder assembly shown in Figure (2-8),which was screwed into the cold end of the refrigerator. Good thermal contact was insured by

the insertion of indium strips between the contact surfaces. The window temperature is monitored by the silicon diode sensor and digital thermometer-controller (Lake-Shore Cryotronics, DRC-7C).

The refrigerator expander and window holder assembly are enclosed in the vacuum shroud shown in Figure (2-9). This shroud was constructed from a standard 2.5 in. Excelon clear PVC tee machined to the dimensions indicated in the figure. Two standard 2.5 in. PVC end caps were machined to accomodate the IR transmission windows, and were cemented to the ends of the straight run of the tee. The two transmission windows were also 1 in. diameter CdTe disks, 0.125 in. thick. The IR radiation from the spectrophotometer enters and exits via these windows. The resultant IR cell/vacuum shroud is simple and inexpensive to construct and enables facile and continuous visual inspection of the sample and the various experimental manipulations. The vacuum shroud is currently evacuated by an Alcatel 2030 mechanical vacuum pump (425 ℓ/min), baffled with a molecular sieve trap. The entire cryogenic refrigerator/vacuum shroud assembly is aligned and positioned in the beam path of a Perkin-Elmer 735B infrared spectrophotometer. The spectrophotometer was calibrated against a standard polystrene sample (Figure 2-10), and in the single beam, calibrate mode on a background water vapor spectrum (Figure 2-11).

Sample gases and/or vapors are admitted to the system via a NUPRO double pattern fine metering valve and 0.125 in. diameter stainless steel tubing. The tubing passes into the vacuum shroud through a 0.125 in. Cajon Utratorr^{R} vacuum fitting tapped into the side of the PVC tee (see Figure 2-8). The tubing terminates at the circumference of the circular opening in the copper window holder (see Figures(2-6,7)), such that the sample gas flows past close and parallel to the window surface. This mode of deposition results in a good even coating of condensate over most of the window area.

REFERENCES

Davidson, N., Statistical Mechanics, McGraw-Hill, N. Y., 1962.

Dushman, S., Scientific Foundations of Vacuum Technique, Wiley, N. Y., 1949.

Liepmann, H. W., Rochke, A., Elements of Gasdynamics, Wiley, N. Y., 1957.

Welsbach, Basic Manual of Applications and Laboratory Ozonation Techniques, Welsbach Ozone Systems Corp., PA. 1977.

TABLE (2.1)

PUMPING SPEED DATA; FIRST TECHNIQUE

Pressure (torr)	Time(s)	$\dot{V}/V_s(s^{-1})$
Experiment 1		
5.9×10^{-6}	0	
4.6×10^{-6}	0.3	1.16
2.7×10^{-6}	0.6	1.85
1.6×10^{-6}	0.9	1.82
0.95×10^{-6}	1.2	1.84
0.55×10^{-6}	1.5	1.61
0.42×10^{-6}	1.8	0.58
0.41×10^{-6}	2.1	
Experiment 2		
4.7×10^{-5}	0	
2.3×10^{-5}	0.3	2.57
1.2×10^{-5}	0.6	2.54
0.55×10^{-5}	0.9	2.58
0.30×10^{-5}	1.2	2.33
0.13×10^{-5}	1.5	3.08
0.06×10^{-5}	1.8	2.67
0.034×10^{-5}	2.1	1.37
0.032×10^{-5}	2.4	
Experiment 3		
7.7×10^{-6}	0	
5.5×10^{-6}	0.3	1.39
3.1×10^{-6}	0.6	2.04
1.7×10^{-6}	0.9	2.06
1.0×10^{-6}	1.2	2.000
0.5×10^{-6}	1.5	2.200
0.34×10^{-6}	1.8	.86
0.33×10^{-6}	2.1	

TABLE (2.2)

PUMPING SPEED DATA; SECOND TECHNIQUE

P_o (torr)	P (torr)	$\dot{V}_{sonic}$ (ℓ/s)	$V_{effusive}$ (ℓ/s)	L_a/d
0.340	2.95×10^{-5}	27.63	16.25	1.20
0.609	4.85×10^{-5}	29.85	17.56	0.68
0.719	5.75×10^{-5}	29.97	17.62	0.57
0.925	7.40×10^{-5}	29.96	17.62	0.44
1.216	1.0×10^{-4}	29.15	17.14	0.34
1.358	1.13×10^{-4}	28.81	16.94	0.30
1.629	1.6×10^{-4}	24.40	14.35	0.25
1.897	1.85×10^{-4}	24.58	14.45	0.22
2.2	2.2×10^{-4}	23.97	14.09	0.19
2.54	2.55×10^{-4}	23.88	14.04	0.16
3.06	3.15×10^{-4}	23.28	13.68	0.13
3.91	4.2×10^{-4}	22.31	13.11	0.10
4.39	4.8×10^{-4}	21.92	12.89	0.09
5.08	5.9×10^{-4}	20.64	12.13	0.08

Figure (2-1). Experimental Apparatus.

KEY:

(1) Mass spectrometer controller

(2) Phase lock amplifier

(3) Oscilliscope

(4) Strip chart recorder

(5) RF/DC generator

(6) NO_x chemiluminescence analyzer

(7) Ozone generator

(8) Ion gauge controller

(9) Digital thermometer/controller

(10) He compressor

(11) Constant head LN_2 reservoir

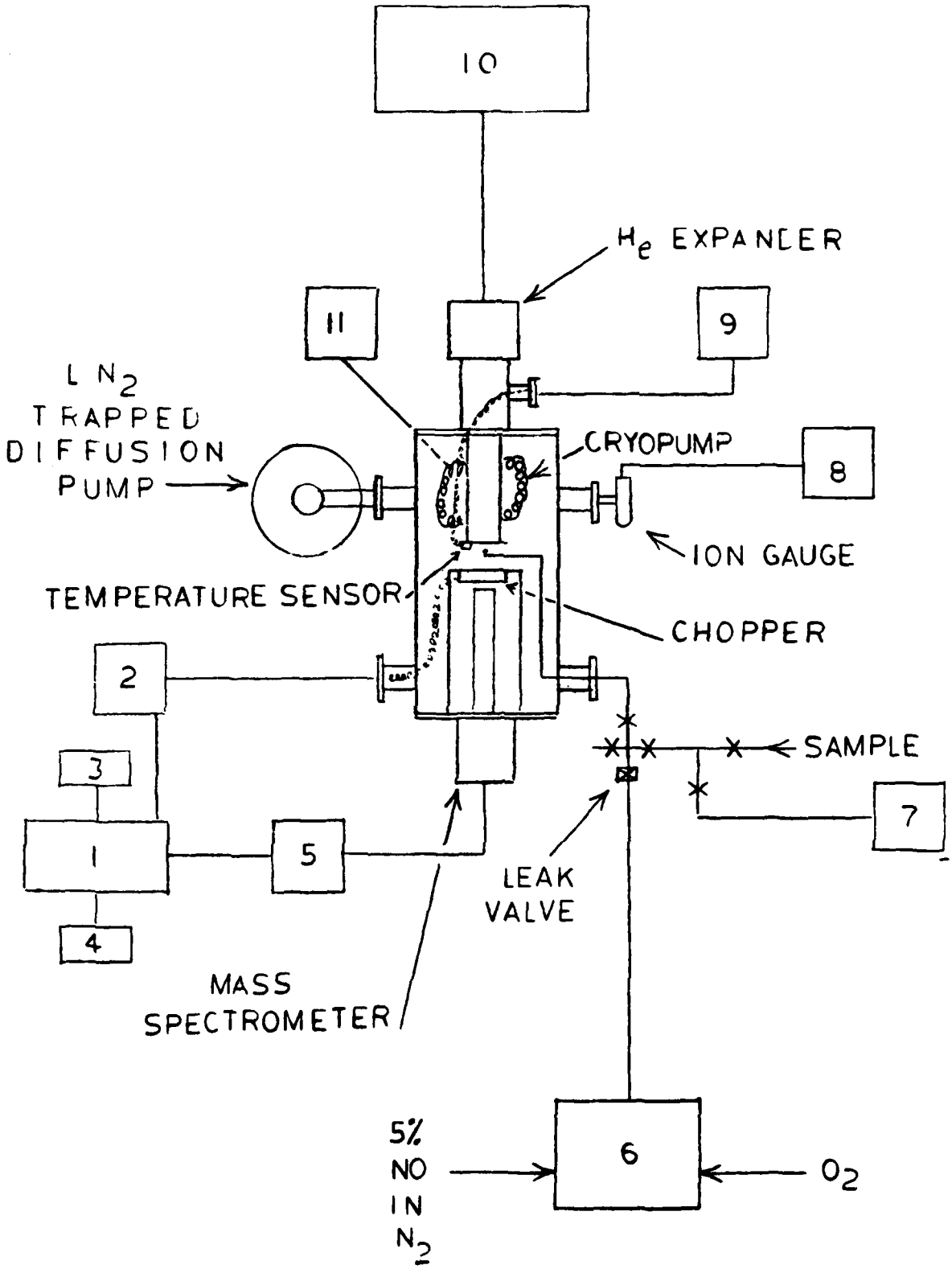
10
He EXPANDER
11
9
LN2
TRAPPED
DIFFUSION
PUMP
CRYOPUMP
8
ION GAUGE
TEMPERATURE SENSOR
CHOPPER
2
SAMPLE
3
7
1
5
LEAK
VALVE
4
MASS
SPECTROMETER
5%
NO
IN
N2
6
O2

Figure (2-1).

Figure(2-2).
Pumping Speed Vs Mean Free Path

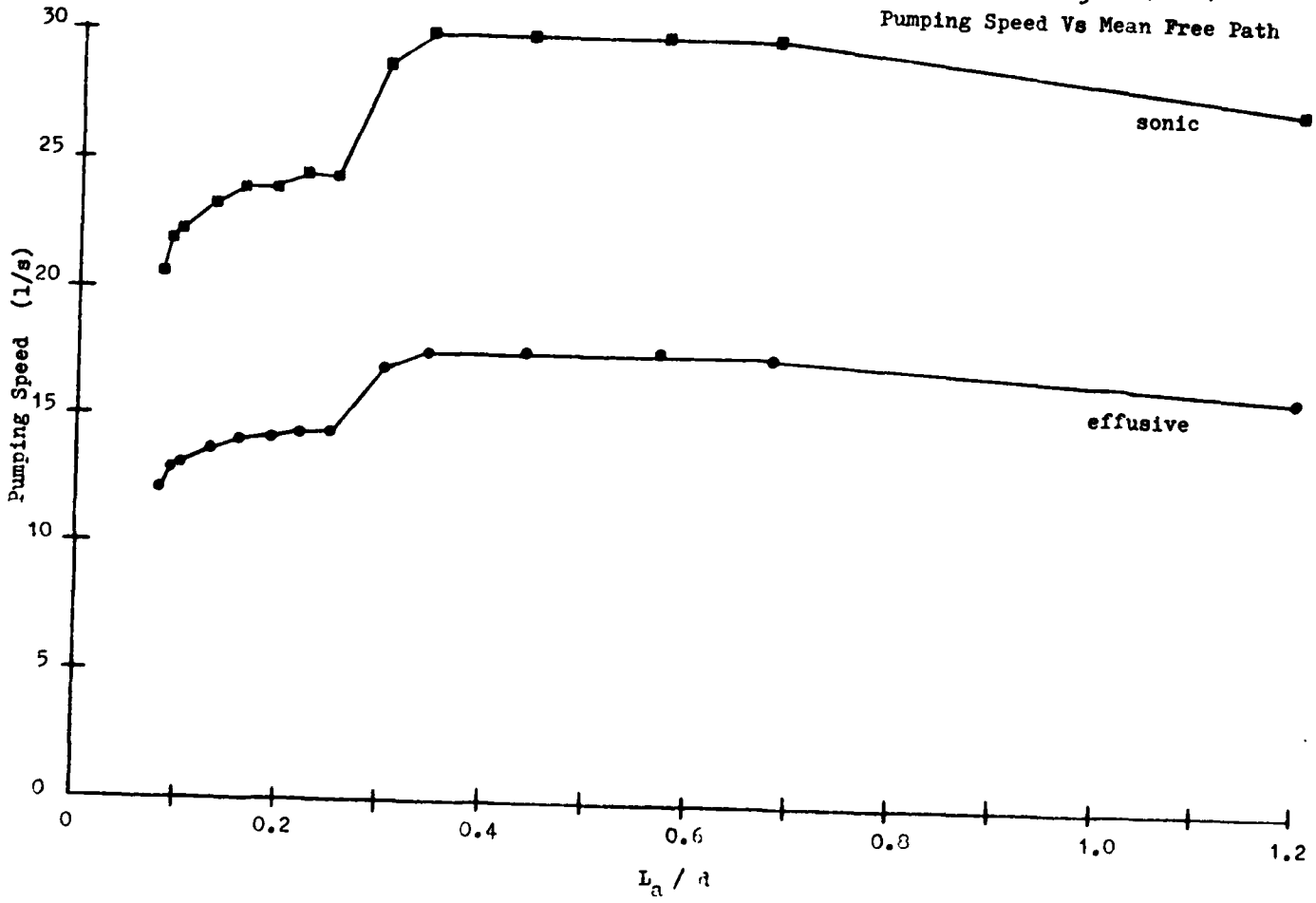

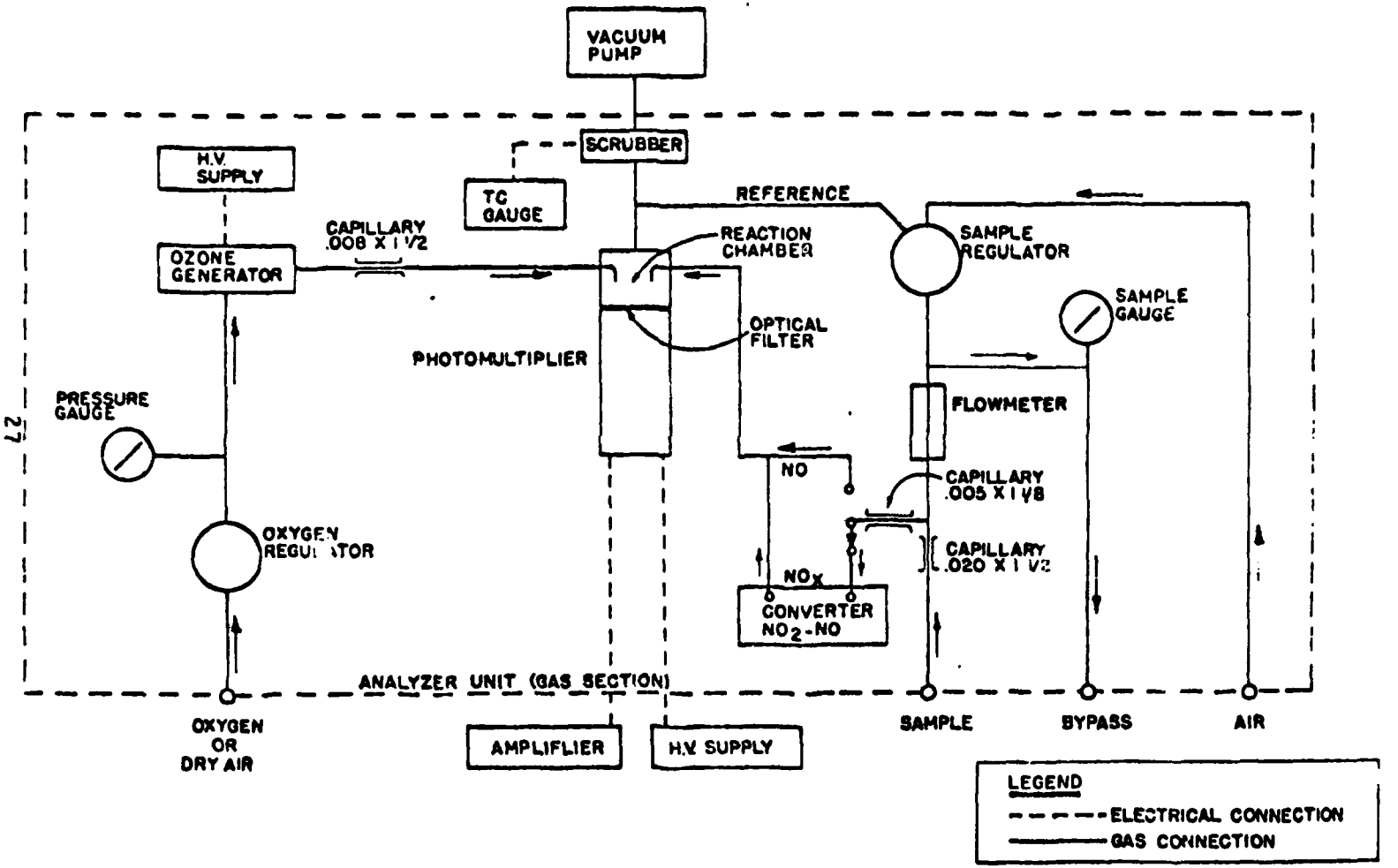

Figure (2-3). NO_x Chemiluminescence Analyzer Flow Diagram
(Reference: Model 10AR Instruction Manual, Thermo Electron Corp., Mass.)

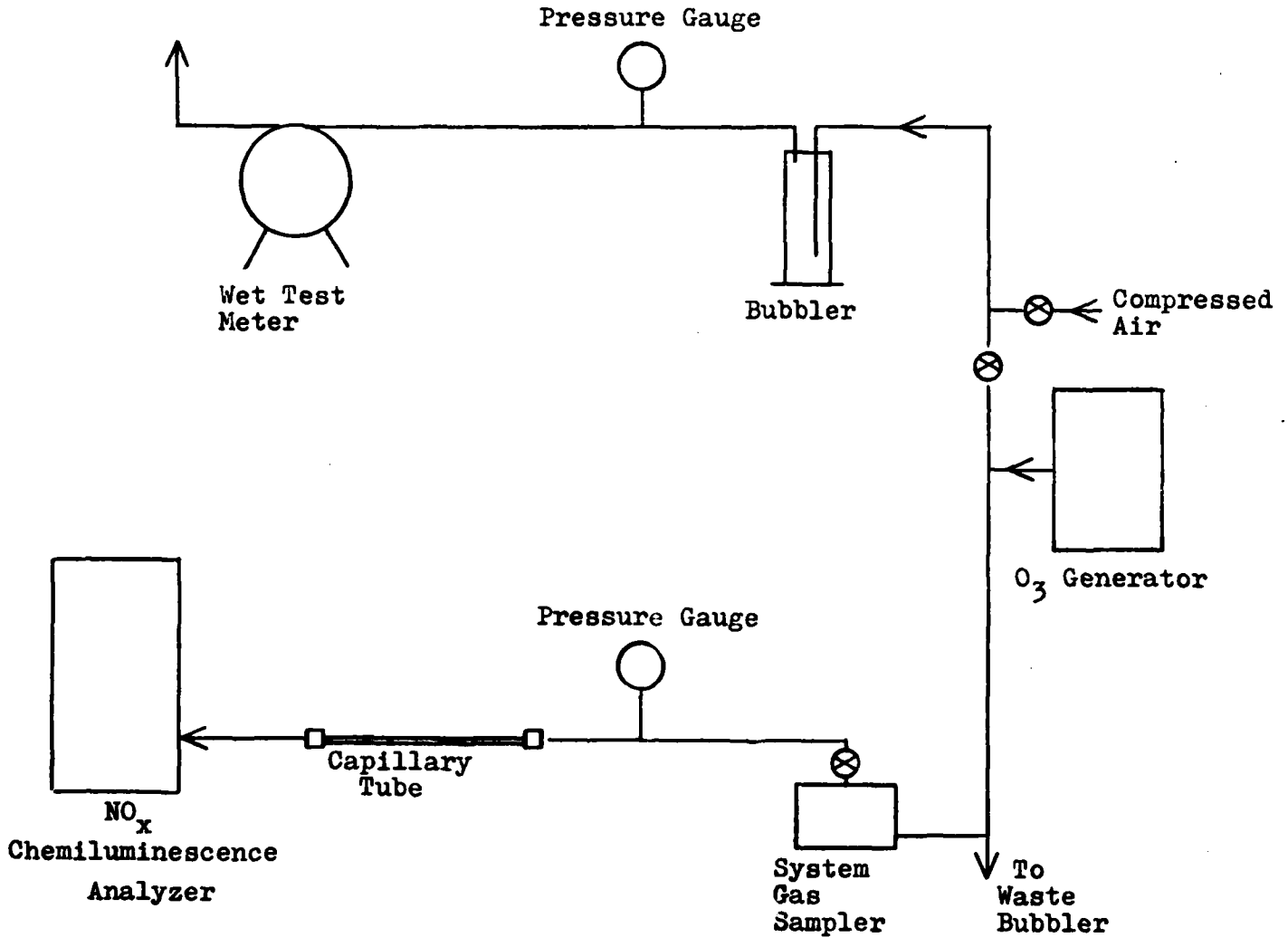

Figure (2-4). Ozone Calibration Apparatus.

Figure (2-5). NO_x Chemiluminescence Analyzer Calibration Curve for Ozone

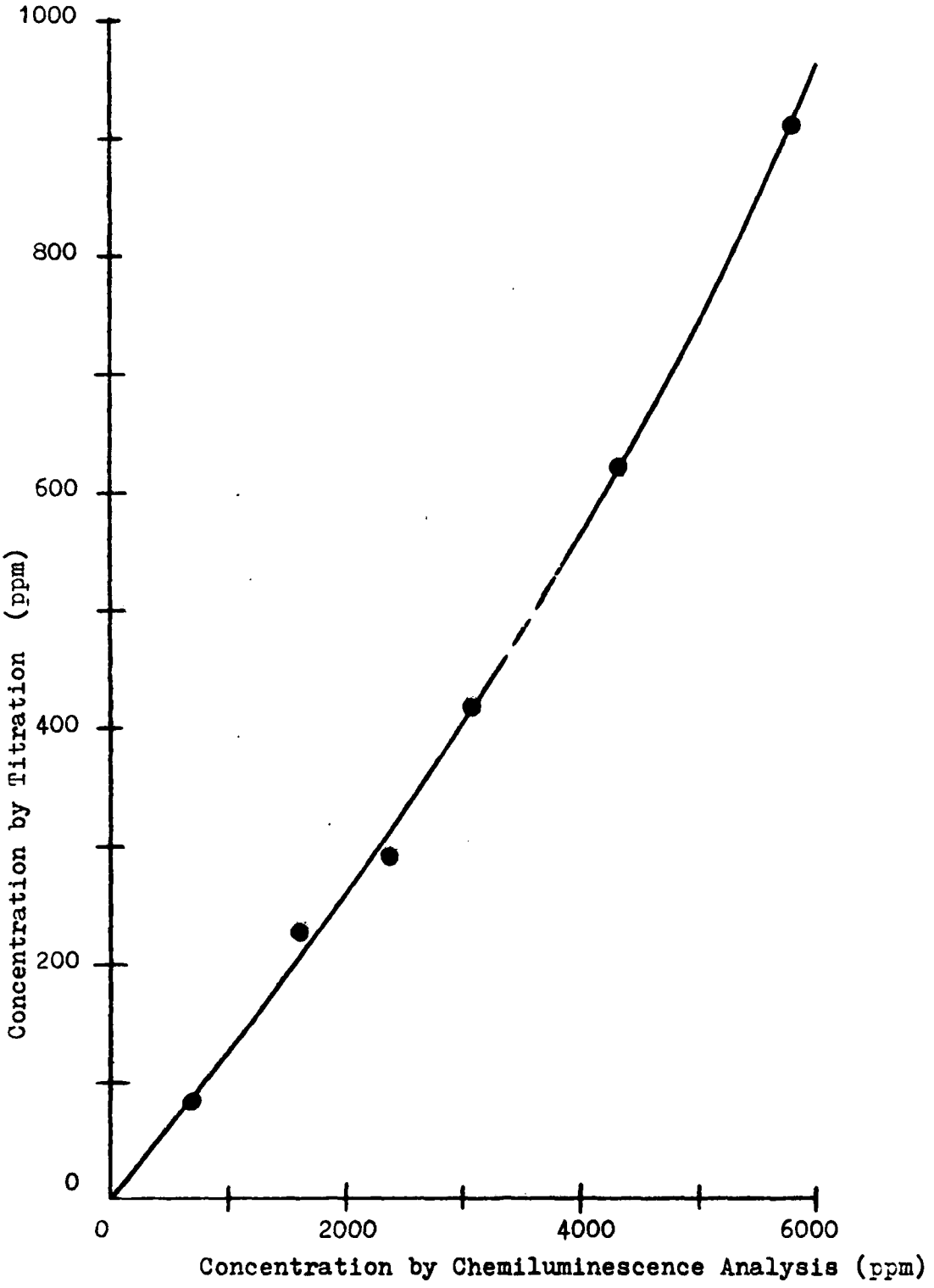

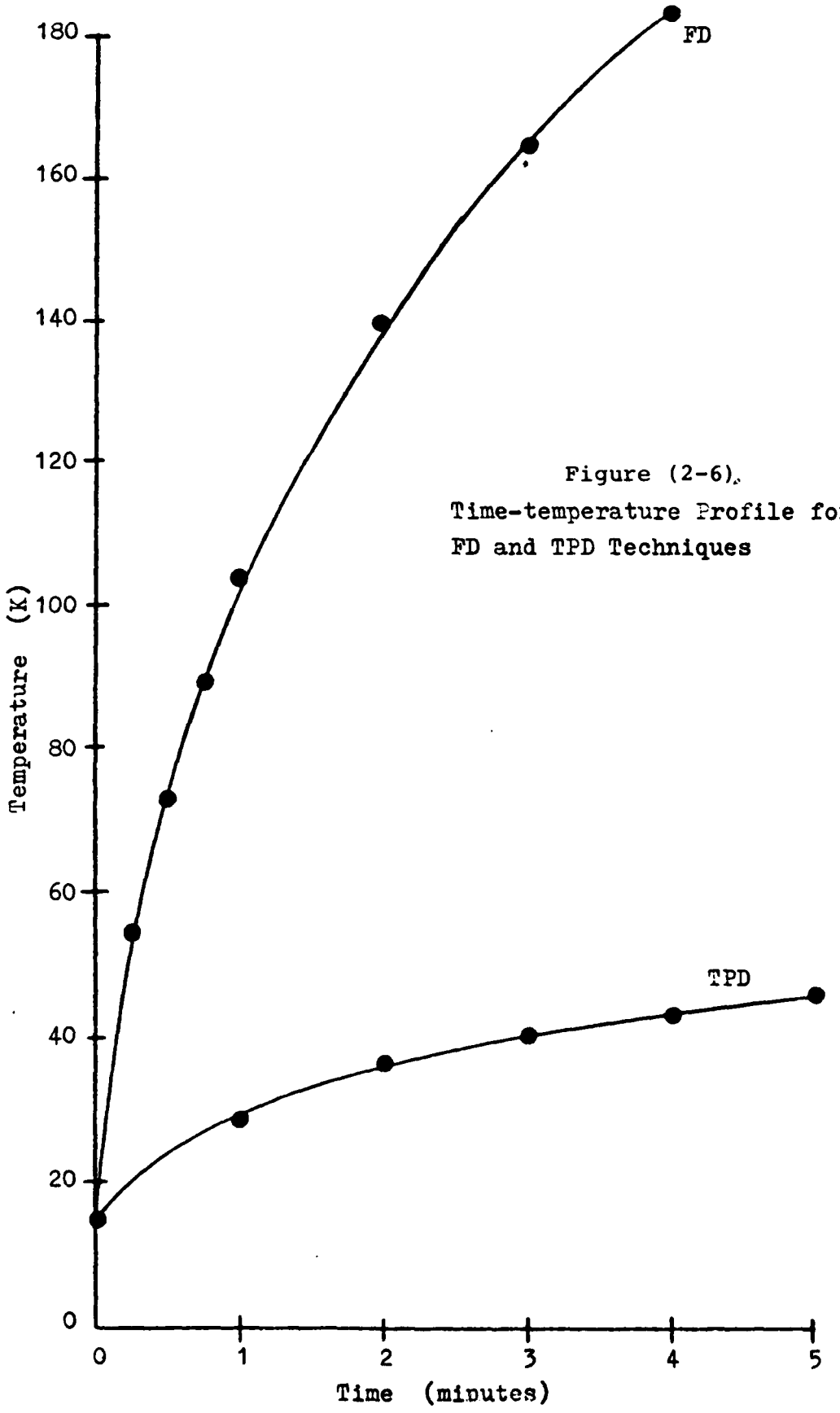

Figure (2-6).
Time-temperature Profile for
FD and TPD Techniques

Figure (2-7). Picture of the IR Spectrophotometry Apparatus.

(A). Perkin-Elmer 735B IR Spectrophotometer (4000-400 cm^{-1}).

(B). Air Products CS202 Displex Cryogenic Refrigerator Expander.

(C). Lake Shore Cryotronics DRC-7C Digital Thermometer/Controller.

(D). Veeco TG-70 Thermocouple Gauge Controller.

(E). Fluke 8022B Digital Multimeter.

(F). Vacuum Line.

(G). Molecular Sieve Trap.

(H). Union Carbide UCON-12 (Freon-12).

(I). Alcatel 2030 Direct Drive Vacuum Pump.

(J). PVC Vacuum Shroud.

(K). Double-Pattern Fine Metering Valve.

(L). CdTe Vacuum Shroud Window (1).

(M). Air Products CS202 Displex Cryogenic Refrigerator Compressor.

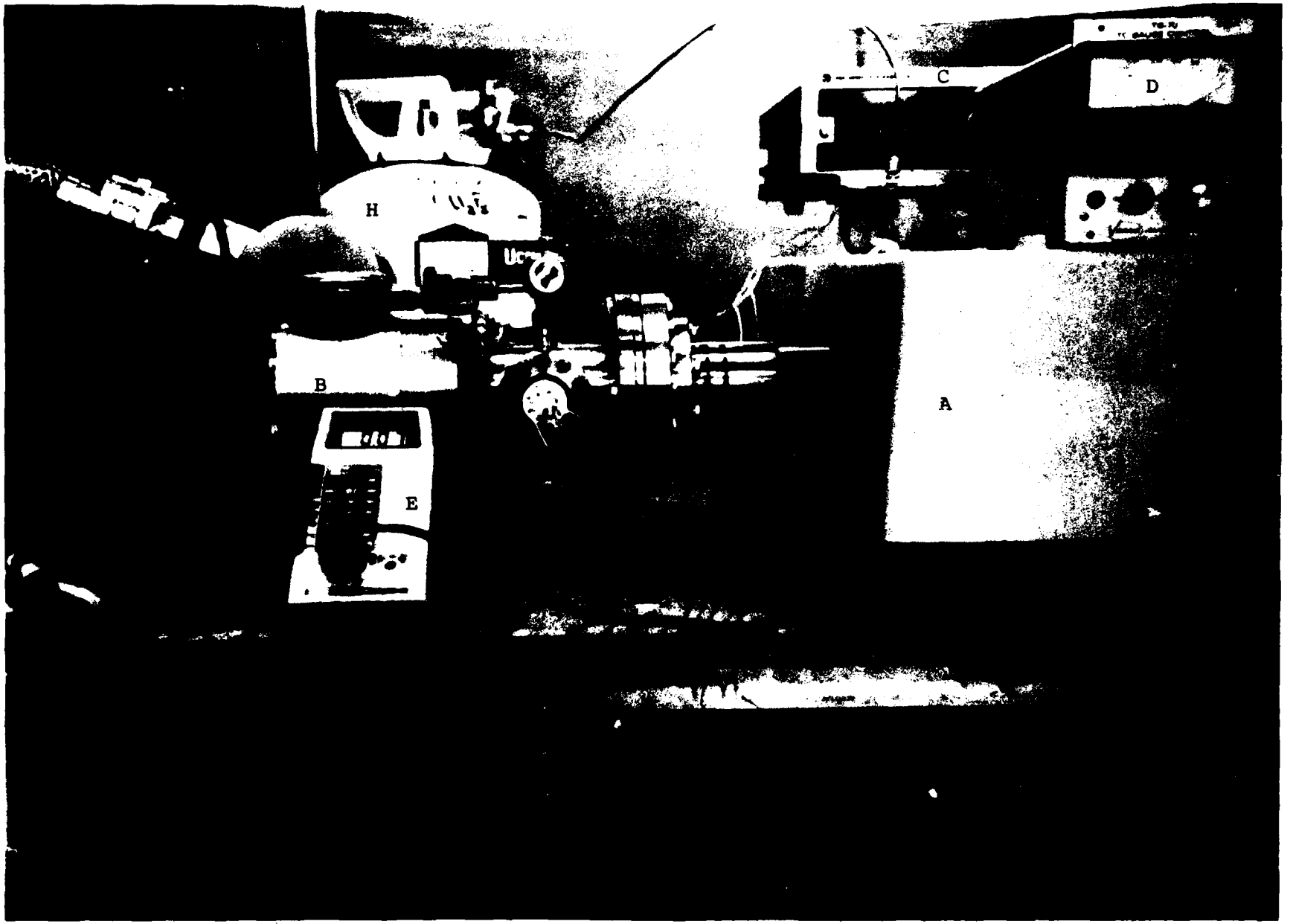

Figure (2-7a).

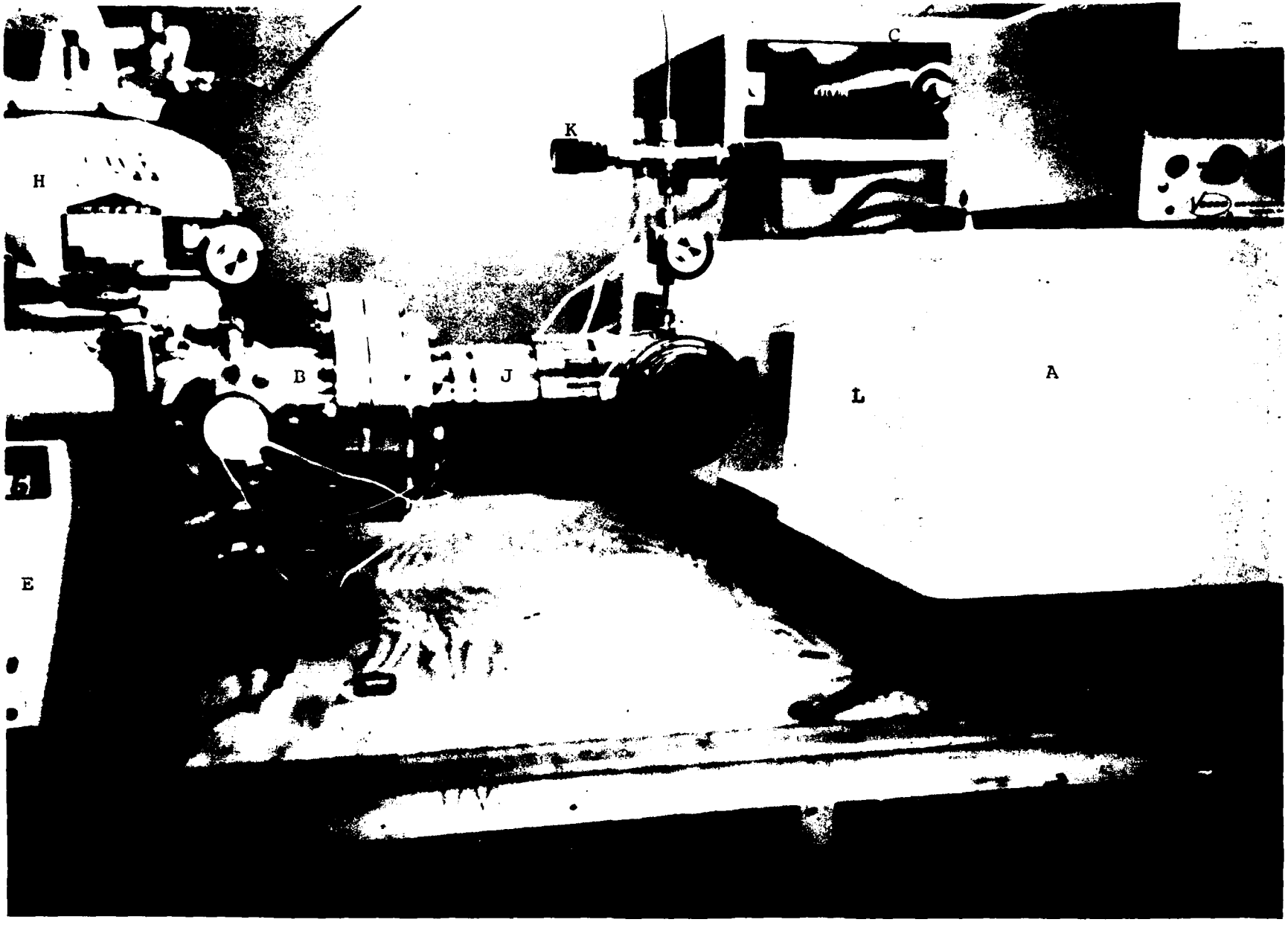

Figure (2-7b)

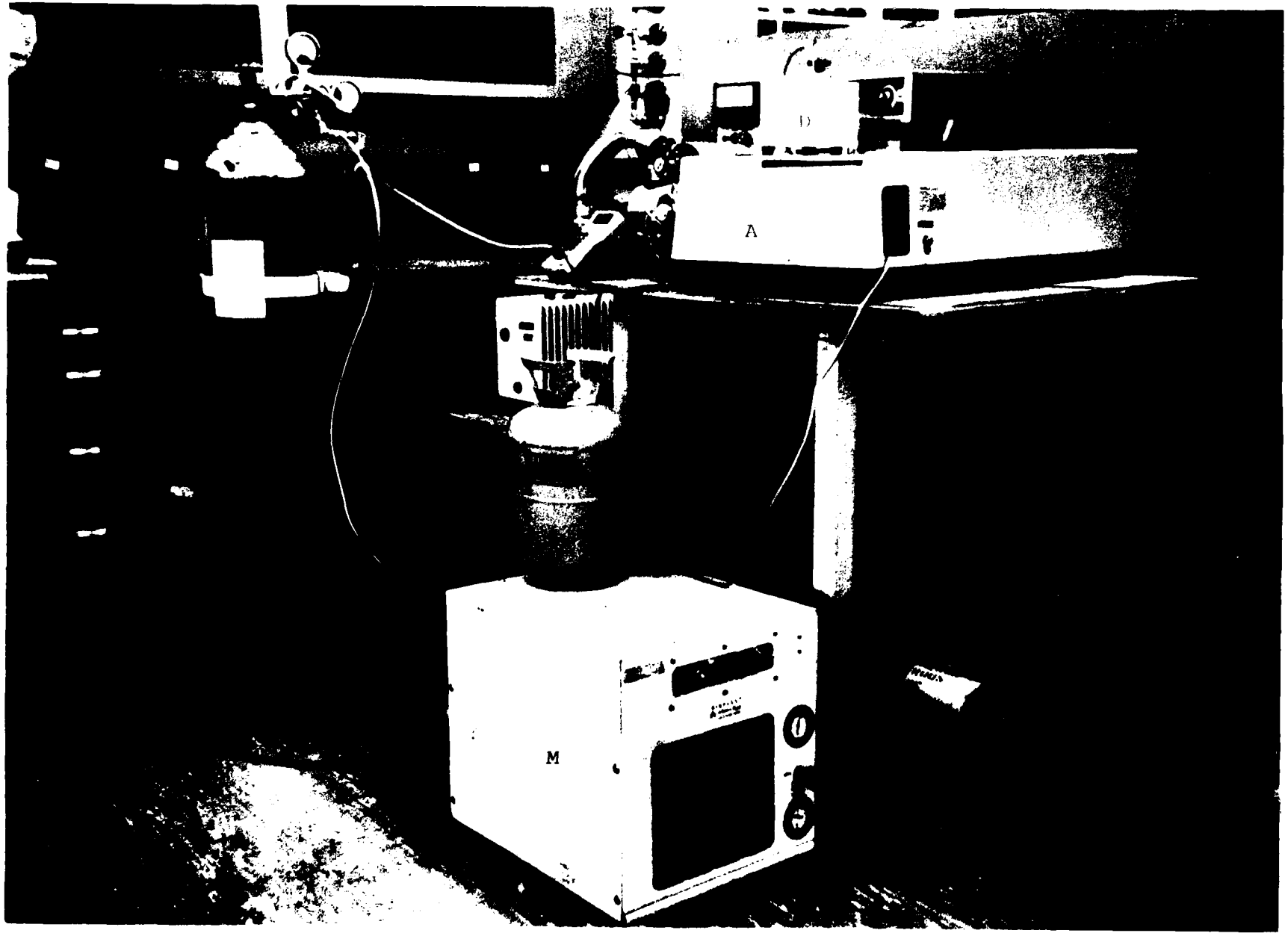

Figure (2-7c)

Figure (2-8). IR Sample Window Holder Assembly.

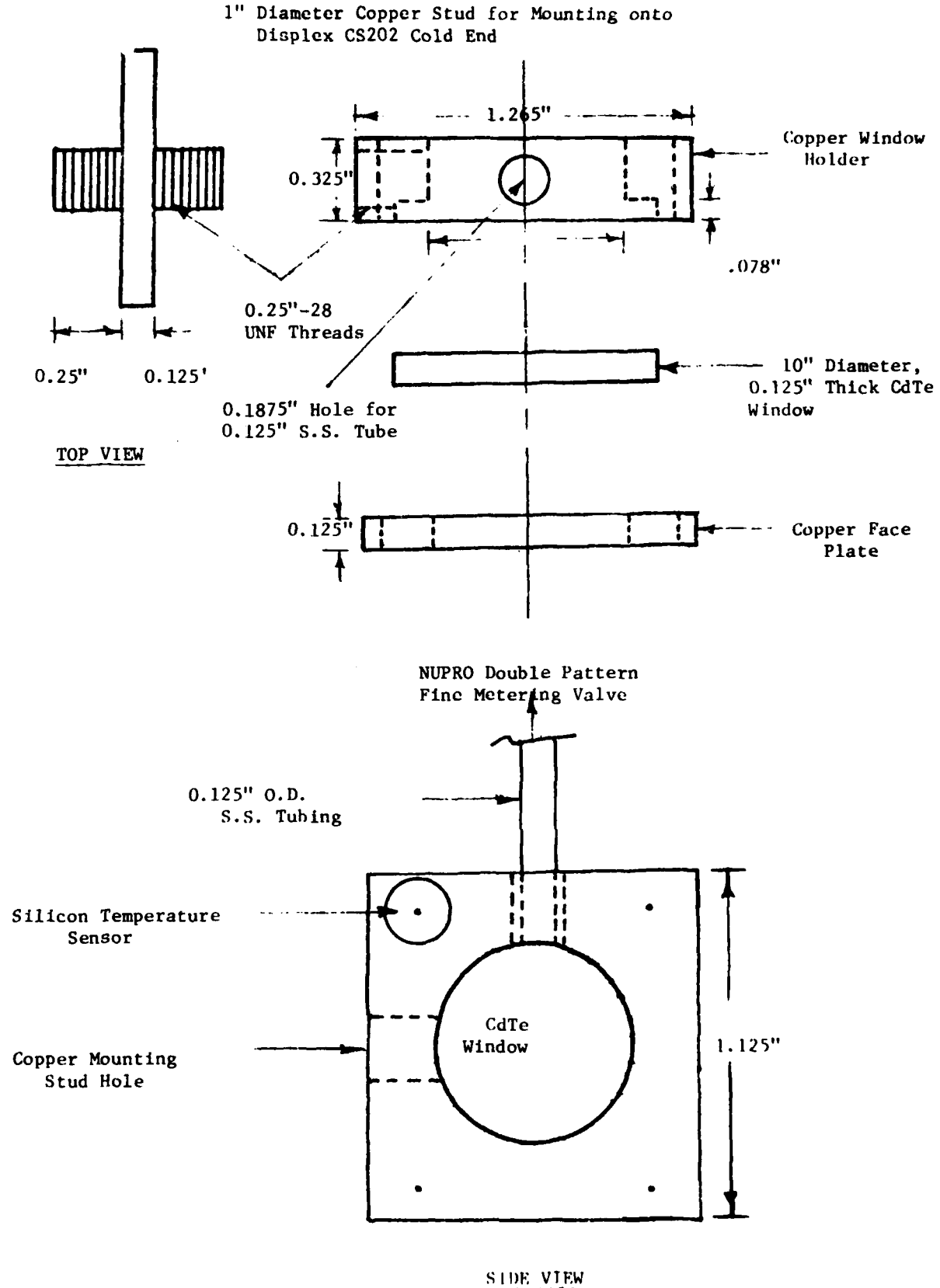

Figure (2-8). IR Sample Window Holder Assembly.

Figure (2-9). PVC Vacuum Shroud Schematic.

Rotatable O-Ring Seal on 2.5" O.D. S.S.
Tube with a 4.5" S.S. Conflat Flange

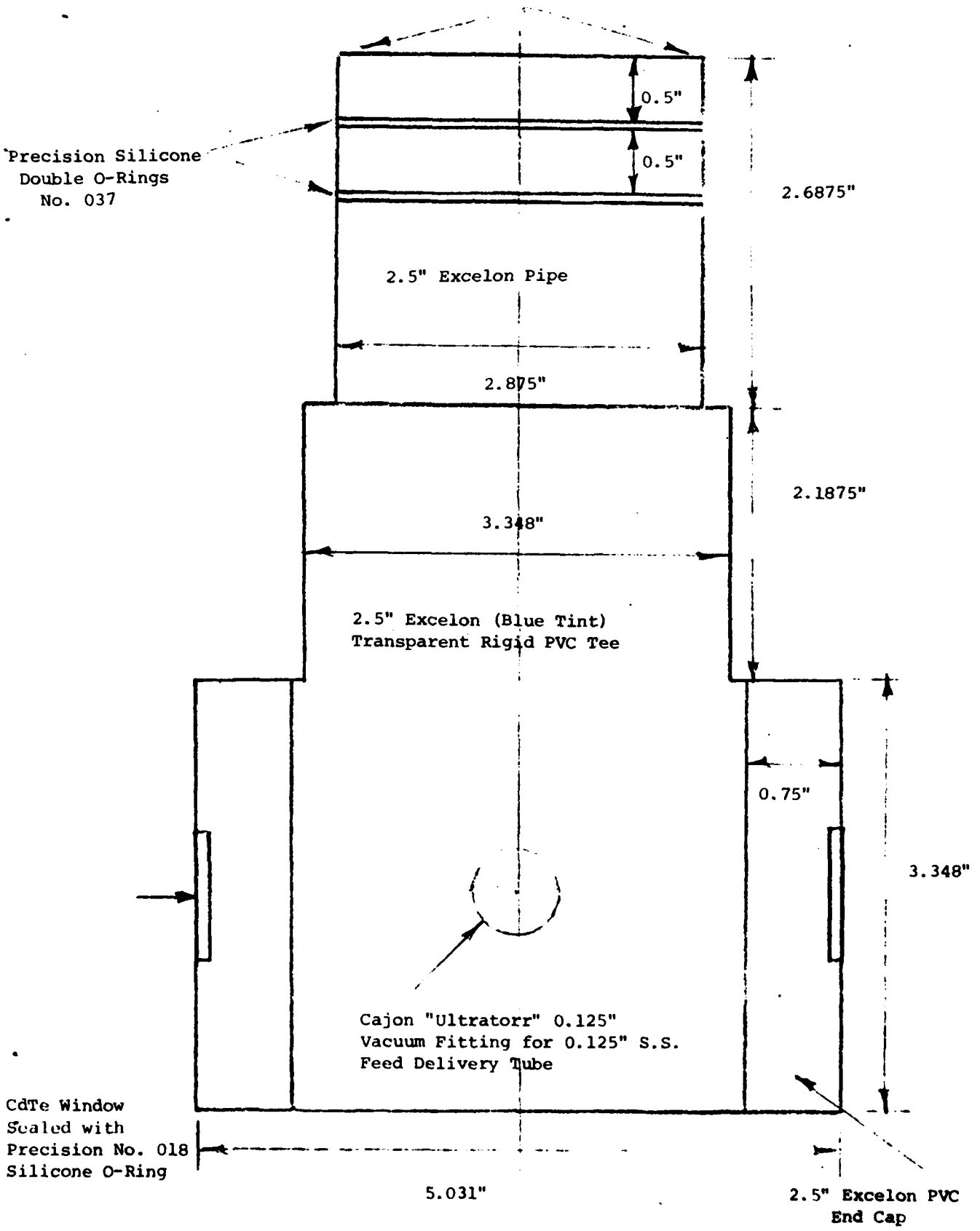

Figure (2-10). IR Spectrum of Standard Polystyrene Calibration Film Inserted Between Vacuum Shroud Window and IR Detector (Cell T=300 K, P=1 mtorr). Inset: Polystyrene Test Spectrum From Perkin-Elmer 735B Instrument Manual.

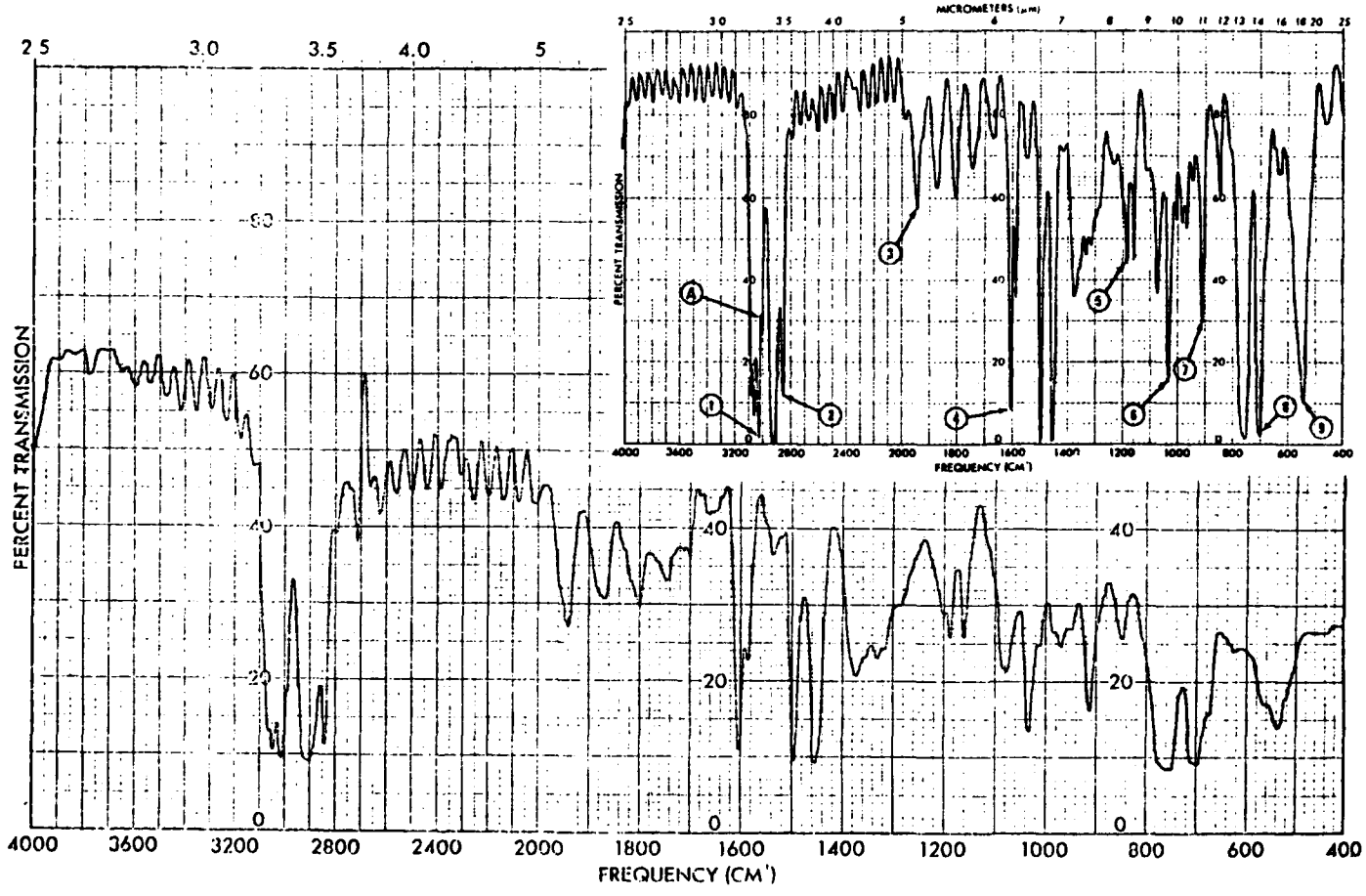
2.5
3.0
3.5
4.0
5
MICROMETERS (μm)
PERCENT TRANSMISSION
60
40
20
0
4000
3600
3200
2800
2400
2000
1800
1600
1400
1200
1000
800
600
400
FREQUENCY (CM⁻¹)

Figure (2-11). Single Beam Background Spectrum With Water Vapor Bands; Calibrate Mode With Nothing in Reference Beam and Sample Beam Blocked. Inset: Same Spectrum From Perkin-Elmer 735B Instrument Manual.

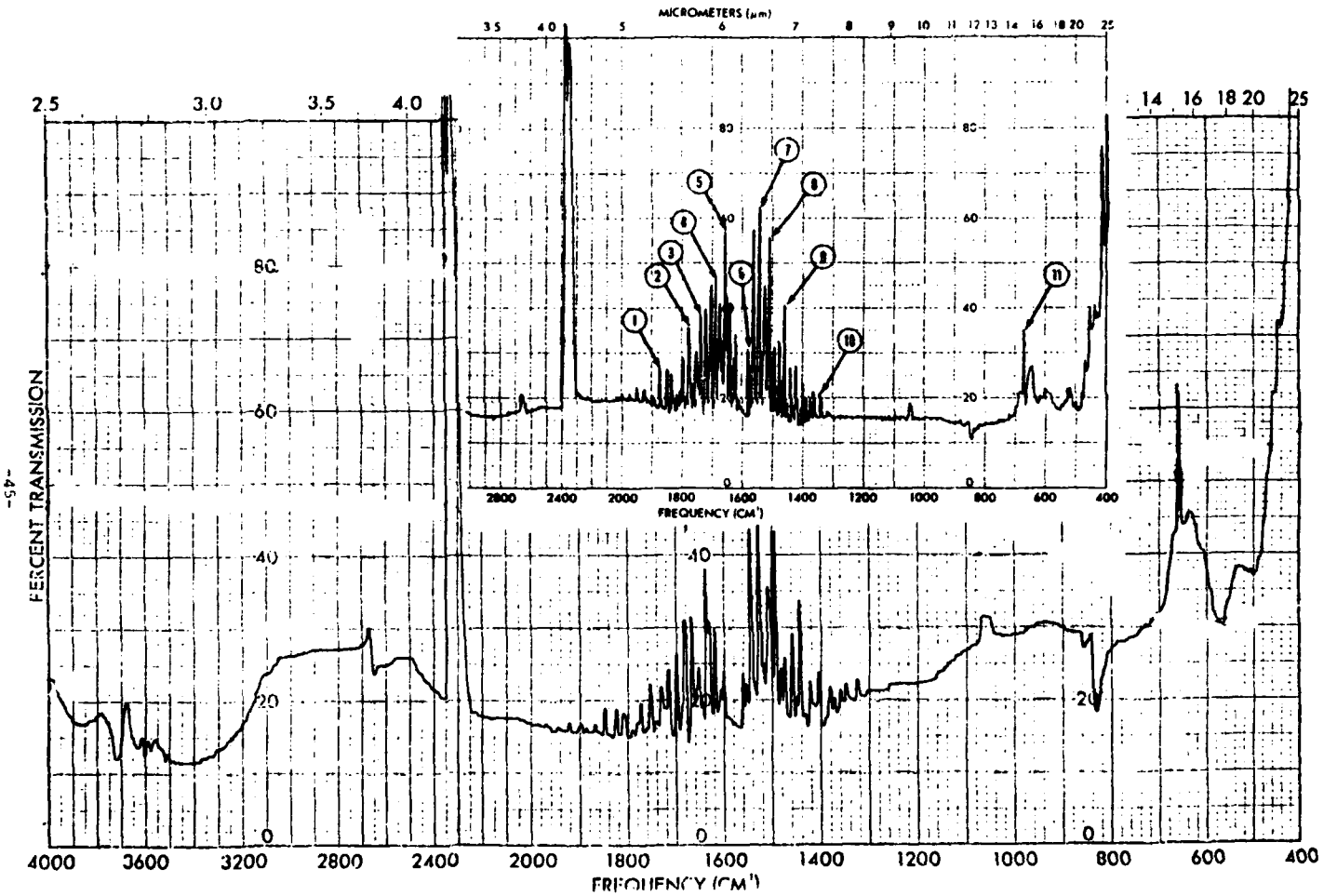
MICROMETERS (μm)
2.5
3.0
3.5
4.0
14
16
18
20
25
PERCENT TRANSMISSION
80
60
40
20
0
4000
3600
3200
2800
2400
2000
1800
1600
1400
1200
1000
800
600
400
FREQUENCY (CM⁻¹)

3. RESULTS AND DISCUSSION

3.1 Desorption Studies

The gold-flashed stainless steel cryosurface was selected for the thermal desorption experiments. This surface was selected both because such surfaces have actually been used in cryogenic whole air sampling flights (Gallagher et. al., 1977, Gallagher and Pieri, 1976), and also because gold is known to be relatively inert catalytically, probably as a result of its filled d-band (Puddephatt, 1978), rendering it incapable of efficiently chemisorbing small molecules (e.g., H_2). Yet some reactions are catalyzed by gold; e.g., partial oxidation of methyl alcohol to formaldehyde (Puddephatt, 1978), and hydrogen-deuterium exchange in some silicon-containing molecules at low temperatures (195-245K) (Bradshaw et. al., 1975). The gaseous species employed in the current studies include N_2, NO, N_2O, CO, CO_2, $CFCl_3$ (F11), CF_2Cl_2 (F12), O_2, and O_3.

The experimental objective is to deposit variable amounts of reactive gases on the gold-flashed, stainless steel surface at 15K, and then desorb the condensed sample in one of two ways. Employing TPD, reactant and product species are monitored with the mass spectrometer. The drawbacks of this technique are limits on total deposit quantity and an inability to accurately detect NO_2 and O_3. The second technique, flash desorption, employs the chemiluminescence analyzer modified and calibrated to detect NO_2, NO, and O_3.

Based upon these results, an extensive set of experiments was conducted to confirm that these observations were not due to contamination of the gases used, or to reactions occurring elsewhere in the system other than in the condensed state on the cryosurface. A summary of the most salient results from these experiments follows.

The nitrogen used to flash desorb the cryofrost (Matheson High Purity, 99.99% min.) was found to contain no NO or NO_x to within the sensitivity of the analyzer (i.e., to 100 ppbv). The NO used (Matheson, certified $\leq$ 0.5% NO_2) was diluted to ca. 100 ppm with the same nitrogen analyzed previously. No deviation at all in the chemiluminescence analyzer reading could be detected in switching between the NO and NO_x modes. Since the 0-100 ppm scale has a detectable accuracy of $\pm$1% of full scale or $\pm$ 1 ppm, this established an upper limit of NO_2 contamination (if any at all) of less than 1%. (Recall that the difference between the NO_x and NO modes for the mixture generated from the cryosurface was a quite substantial 61 ppm. In order to account for this result in terms of NO_2 contamination of the pure NO, the sample gas had to be 46% NO_2--considerably in excess of the 1% detection limit.)

In order to check that NO_2 was not being generated on the walls of the feed system or on the vacuum chamber walls, the 0.5% NO in N_2 calibration standard (Matheson, certified) was fed to the sealed-off vacuum system with the cryosurface at room temperature to a total pressure of 0.5 atm, and then brought up to atmosphere pressure with pure nitrogen. Subsequent chemiluminescence analysis of the resultant mixture

yielded no difference between the NO and NO_x mode readings (i.e., 2500 ppm in both cases). Consequently, no detectable NO_2 was formed in the system under conditions similar to the reactive experiments except that no NO was allowed to condense on the cryosurface. It was, therefore, concluded that the reaction is indeed genuine and that it is a direct result of the condensation and desorption processes.

To our knowledge, these results represent the first observations of NO self-disproportionation from the solid state in the absence of a porous adsorbent. The only other observations we are aware of which are even somewhat similar are those of Addison and Barrer (1955). These workers observed NO disproportionation to near completion after adsorption on zeolites at low temperatures via:

$$4NO \rightarrow N_2O + N_2O_3 \qquad (R1)$$

$$3NO \rightarrow N_2O + NO_2 \qquad (R2)$$

When charcoal was used as the adsorbent for NO condensed at low temperatures, considerable evolution of NO_2 was detected upon thermal desorption and the reactions:

$$4NO \rightarrow N_2 + 2NO_2 \qquad (R3)$$

$$6NO \rightarrow N_2 + N_2O_3 \qquad (R4)$$

were suggested (Addison and Barrer, 1955). Yet a blank experiment (i.e., condensation of NO for 100 hrs. at -183°C with no adsorbent) yielded no detectable levels of disproportionation products. In this work disproportionation was attributed to catalytic activity of the porous adsorbent.

This technique allows a faster desorption time and high dilution in the gas phase. Its limitations are that it is specific to these three species only, and that a minimum sample size must be deposited in order to insure that the final sample gas concentration is within the detectable limits of the chemiluminescence analyzer. Thus these two methods are, in a sense, complementary.

3.1-1. NO Disproportionation

Deposition of NO on the gold-flashed cryogenic surface, followed by temperature programmed desorption (TPD) or flash desorption (FD) with pure nitrogen, revealed a surprisingly strong and persistent disproportionation reaction. For example, in one such experiment 3.5×10^{-7} g mol of NO was steadily deposited on a 15 K gold-flashed stainless steel cryosurface (i.e., condensing the entire beam) for five minutes, yielding a total deposit of 1.1×10^{-4} g mol of NO. After approximately three minutes, the NO cryodeposit was flash desorbed with pure nitrogen; i.e., the entire deposit was rapidly desorbed into the gas phase with room temperature nitrogen admitted to the vacuum chamber to a final pressure of 136 kPa such that no condensate remained on the surface. The resultant diluted concentration of NO in nitrogen should have been approximately 215 ppm. The actual results by chemiluminescence analysis were quite different, yielding 72 ppm NO and 133 ppm NO_x, or $NO/NO_x = 0.54$. Thus, about two-thirds of the NO originally deposited was converted to higher oxides of nitrogen in the absence of any oxygen (O_x) species.

Due to the significant levels of NO_2 detected in our own experiments, the stoichiometry of (R3) was investigated further using a different experimental technique -- thermal desorption with mass spectrometric detection (n.b., not flash desorption with pure nitrogen). Thermal desorption of a pure NO cryofrost while monitoring mass peak m/e = 28 yielded the desorption spectrum presented in Figure 3-1. (n.b., no nitrogen was used in these experiments.) Assuming, for the moment, that the two peaks observed are due to nitrogen as a disproportionation product, integration of the spectrum yields approximately 9.8×10^{-7} g mol N_2 generated. Knowing that 8.8×10^{-6} g mol of NO were originally deposited in this experiment, and assuming that the stoichiometry of (R3) holds, implies that 1.96×10^{-6} g mol of NO_2 should also have been formed such that the final $NO/NO_x \cong 0.71$. This latter value compares quite favorably with the NO/NO_x ratio of 0.54 for the previous flash desorption experiments. Differences in the experimental techniques (flash desorption vs. thermal desorption), and analytical techniques (chemiluminescence vs. mass spectrometry), and absolute quantities deposited could account for the differences in conversions actually observed. Therefore, the stoichiometry of (R3) accounts for at least a major fraction of the NO disproportionation. The slightly higher conversions detected directly in the flash desorption experiments with chemiluminescence may imply that (R3) is not the only reaction that occurs. However, the fact that no trace of the parent peaks of the nitrogen oxides N_2O and N_2O_3 could be detected with

the mass spectrometer upon thermal desorption, leads us to conclude that the primary products of disproportionation in our system are indeed nitrogen and nitrogen dioxide (i.e., (R3)). Thus, the reactions suggested by (R1), (R2), and (R4), if they occur at all, must be significantly less important in our system.

Although not discussed here, the thermal desorption spectrum of pure condensed nitrogen is quite different from that indicated in Figure 3-1; i.e., pure nitrogen desorbs from the gold-flashed stainless steel cryosurface in three, closely grouped peaks appearing in the 28-40 K range. This strongly suggests then that the nitrogen peaks at 64 K and 82 K in Figure 3-1 are due to spontaneous nitrogen generation at these temperatures during the desorption process. This is supported by the mass peak m/e = 30 desorption spectrum for pure NO presented in Figure 3-2. As shown, the 64 K and 82 K desorption peaks of nitrogen in Figure 3-1 correspond quite closely to the two major mass 30 desorption peaks in Figure 3-2. (Since mass 30 is also a fragment of NO_2 in the mass spectrometer, the fraction of either or both of the two peaks in Figure 4 attributable to NO_2 vs. NO could not be determined). This mechanism is consistent with the observations of Addison and Barrer (1955) who suspected that NO disproportionation on zeolites also occurred during the thermal desorption process.

In the present work, it is quite possible that NO disproportionation is self-catalyzed by its own frost. Abe and

Schultz (1979) have shown that rare gases deposited at intensities of approximately 5×10^{20} $m^{-2}s^{-1}$ onto low temperature (4.22K) surfaces are quite porous. These conditions correspond closely to those in the present work (e.g., 10^{18} -10^{21} $m^{-2}s^{-1}$ and 15 K). Although the pore structure probably decomposes somewhat during heating to desorption, sufficient structure could remain to provide a stabilizing environment for reaction intermediates. In addition, the frost provides a source of highly concentrated NO in the proximity required for the four-center reaction suggested by the stoichiometry of (R3). An estimate of the heat of reaction of (R3) in the solid phase at 50 K from thermodynamic data (Reid et al., 1977, and Dean, 1973) yields -64 kcal/g mol. The exothermicity of this reaction is sufficient to provide enough energy to allow the reaction to proceed via a chain reaction mechanism. The absence of heat transfer limitations (i.e., the energy liberated is transferred directly to other potential reactants) would tend to make this an extremely rapid process.

3.1-2. Attempts at NO_x Disproportionation Inhibition

One objective of our work was to study the possible oxidation of NO by O_3 during the deposition and desorption process. The disproportionation reaction makes such studies difficult by masking the production of NO_2 by oxidation with the NO_2 produced via the self-disproportionation mechanism. In an attempt to eliminate this undesired reaction, matrix isolation was attempted. (Matrix isolation techniques have been reviewed by Cradock and Hinchcliffe (1975), Hallam and Scrimshaw (1973) and Meyer (1971)).

In one experiment 1.4×10^{-3} g mol of a 5% NO in N_2 gas mixture (NO = 7×10^{-5} g mol) were deposited and subsequently flash desorbed with N_2. The resulting NO/NO_x ratio of 0.5, found by chemiluminescence confirmed that matrix isolation by N_2 did not effectively reduce the conversion due to disproportionation.

A TPD spectrum for m/e = 28 obtained upon the desorption of approximately 5×10^{-6} g mol of the 5% NO in N_2 mixture (2.5×10^{-7} g mol of NO) deposited at 15K, is presented in Figure 3-3. This spectrum shows that the vast majority of N_2 desorbs by 50K. In a companion experiment, the same amount and type of deposit was desorbed except that the NO parent peak (m/e = 30) was monitored. The resultant desorption curve is presented in Figure 3-4. The low level carryover of NO during the desorption of N_2 in the 20-45K range (shown in Figure 3-3) and the subsequent drop in NO signal at approximately 42K, signaling the end of NO carryover by desorbing N_2, are noted. Thus, it seems that N_2 phase separates from NO and desorbs with little quantitative carryover of NO, although they were initially well mixed, leaving essentially pure NO on the cryosurface. Figure (3-4) also exhibits the characteristic NO peaks in the 64K and 82K temperature ranges, as in Figure (3-2) for pure NO. Thus once the N_2 matrix desorbs the remaining NO desorbs essentially as pure material.

In Figure (3-3) there is evidence of low levels of N_2 production at 82K, even though mass 28 background levels are

relatively high. Along with the FD data cited previously, this shows that matrix isolation of NO in N_2 at this concentration (5%) is ineffective in totally inhibiting the disproportionation reaction; i.e., N_2 phase separates and desorbs first, leaving pure NO on the surface. Therefore, carbon dioxide was chosen as a matrix material due to its low vapor pressure in comparison to NO, which allows it to remain rigid and to continue to isolate NO above its normal desorption temperature (Redhead et al., 1968, Honig and Hook, 1960). (The vapor pressure of CO_2 is 10^{-5} torr at 91.5K, while for NO, the vapor pressure is 10^{-5} torr at 57.6K.) Thus the CO_2 matrix should survive at temperatures above the point at which NO first desorbs. Cradock and Hinchcliffe (1975) define the onset of cryofrost annealing to occur (discussed subsequently) at 30% to 50% of the normal melting point, which is 216.6K for CO_2 (Hallam and Scrimshaw, 1973). Thus the CO_2 matrix should begin to lose rigidity between 65K and 108K.

To test this theory at high concentrations, 3.3×10^{-4} g mol of a 30.5% mixture of NO in CO_2 were deposited on the 15K cryosurface and then flash desorbed with N_2. This procedure resulted in a NO/NO_x ratio of 0.41, which is somewhat lower than previous results, implying an even more effective disproportionation conversion. In another experiment, 5.7×10^{-4} g mol of 8.2% NO in CO_2 were deposited on the 15K cryosurface and flash desorbed. The results were quite similar

to the more concentrated case; i.e., an NO/NO_x ratio of 0.42 was found. Thus lowering the concentration of NO in the CO_2 by more than a factor of three had little effect on conversion due to disproportionation. Thus it must be concluded that matrix isolation is not effective at these dilution ratios during the desorption process. It is possible, as evidenced by the NO/NO_x ratios, that the CO_2 matrix acts as superior catalyst for NO disproportionation than does pure NO. Thus TPD experiments employing 8.2% NO in CO_2 were performed to determine if matrix isolation in CO_2 has any effect.

In one experiment, approximately 1.3×10^{-5} g mol of 8.2% NO in CO_2 were deposited and then desorbed by TPD, while monitoring mass 30. A companion experiment was conducted with the same gas sample except that mass 44 was monitored for CO_2 desorption. In yet another experiment, 10^{-5} g mol of pure CO_2 were deposited, and mass 44 was monitored. The results of these three experiments are presented in Figure (3-5), where curve A is the desorption pattern of NO in the $NO-CO_2$ mixture, curve B is the desorption pattern of CO_2 in the $NO-CO_2$ mixture at lower deposit quantities, and curve C is the desorption pattern of pure CO_2. Note that curves B and C show that the CO_2 desorbed from the $NO-CO_2$ mixture begins to peak at the same temperature as pure CO_2, but that the peak width is narrower, due to the small amount of CO_2 desorbed. Thus the CO_2 behavior is unaffected by the NO in the matrix.

The nature of the desorption pattern of NO from the $NO-CO_2$

mixture, as illustrated in curve A of Figure (3-5), is substantially different from the desorption spectra of pure NO shown in Figure (3-2), which exhibits two maxima of nearly equal area, at 66K and 83K. In Figure 3-5 of matrix-isolated NO, the low temperature (63K) peak has an area approximately two orders of magnitude less than the higher temperature peak, which is shifted to approximately 88K, coincident with the CO_2 desorption temperature. Thus the attempted matrix isolation in CO_2 was partially successful in that a major desorption peak of pure NO at 66K was reduced substantially (and shifted slightly), trapping the NO in the CO_2 matrix until that matrix began to sublimate, resulting in a wider desorption peak at 88K, corresponding approximately to both NO and CO_2 desorption. Thus a low vapor pressure matrix material can trap the more volatile NO. Yet, flash desorption experiments show that this effect does not stop disproportionation. Thus aggregation of NO must occur prior to desorption, if the solid phase disproportionation theory is correct. Reasons why this technique did not stop the disproportionation reaction are discussed below.

The term matrix isolation is actually a misnomer for the effect sought in the present work. It has been shown that disproportionation occurs just before or during the desorption of NO, according to the N_2 byproduct desorption peaks. In classic matrix isolation experiments, reactions are minimized by careful control of the matrix temperature, and thereby the diffusivities or mobilities of the reacting constituents. These conditions are clearly not met here, where the

cryofrost is heated to complete desorption. Cradock and Hinchcliffe (1975) have shown that the probability of CO in a rare gas matrix being completely isolated (i.e., no CO nearest neighbors) is given by $(1-r)^{12}$ for CO isolated in a matrix with 12 nearest neighbors, where r is the inverse of the matrix ratio (r = moles solute/moles solvent). Complete isolation is even more difficult when the trapped species interacts strongly with the matrix material. Thus a matrix containing NO:CO_2 as 1:100 would only have 88.6% of the NO completely isolated. In the present case the ratio is $(1-(8.2/91.8))^{12}=0.325$, and thus approximately 67.5% of the NO in the NO:CO_2 mixture deposited as cryofrost has NO as a nearest neighbor. Thus, most of the NO interacts with other NO molecules.

In order to achieve true isolation, much higher dilution ratios are necessary. A matrix ratio of 1000 (solvent/solute) provides 98.8% isolation of solute species, while a matrix ratio of 10,000 provides 99.9% isolation. These higher dilution rates are impractical for both TPD and FD experiments in the current work. For TPD-type desorption, the absolute quantity deposited is limited by the vacuum system pumping speed. Thus small quantities of highly dilute sample render solute desorption spectra practically impossible to detect above background levels.

In the case of flash desorption type experiments, deposition times on the order of several days would be necessary to deposit enough solute to be detected employing chemiluminescence analysis. Thus for true matrix isolation

type experiments, a surface specific analysis technique such as IR (Hallam and Scrimshaw, 1973, Meyer, 1971) becomes a necessity.

The basic purpose of the "matrix isolation" experiments performed here was to determine the effect of dilution of NO by CO_2 in a range appropriate to the limits of the current experimental system. Since a four-NO molecule aggregate is believed to be the minimum size necessary for disproportionation, dilutions in the ranges feasible for the current apparatus should have induced at least some reduction of the extent of reaction.

During deposition of the cryofrost, care must be taken in controlling the deposition rate. If the rate becomes too high, local hot spots may develop due to poor thermal conduction to the refrigerator heat sink for the heat of sublimation, and local diffusion and aggregate formation can occur. Cradock and Hinchcliffe (1975) recommend a deposition rate of 18 mg mol/hr. as the rate that best balances the diffusion problem against opacity problems associated with very low growth rates (although IR transmittance is not a problem here), while Meyer (1971) recommends a rate of 1 to 2 mg mol/hr. In the present work, the maximum deposition rate was approximately 2 mg mol/hr. for flash desorption experiments and 0.1 mg mol/hr. for TPD type experiments. Though these rates would seem to comply with those recommended, there is evidence that NO may be more sensitive to aggregate formation during deposition. For example, Varetti and Pimentel (1971) reported that in studies

of highly dilute matrices of NO and NO_2 in N_2 ($N_2/(NO+NO_2)=500$) deposited on a 20K surface at 10 mg mol/hr., IR bands of NO dimers and higher aggregates were readily observed. Since the high NO concentration in matrices in the present work require a substantially shorter diffusion path to aggregate, aggregation of NO during deposition is a distinct possibility. However, a technique such as IR spectrophotometry would be required to unequivocally confirm this conjecture. Thus, it seems that the working concentration range in the current work is too high to prevent dimerization, and that matrix deposition probably leads to aggregate formation.

The process of thermal desorption causes a considerable degree of diffusion in the frost. In matrix isolation studies, diffusion in matrices is usually treated in terms of matrix rigidity. Cradock and Hinchcliffe (1975) note the common rule of thumb for matrix rigidity: viz., below $0.3T_m$ (where T_m is the normal melting point), the matrix is considered rigid; i.e., it remains essentially in its initial state, as formed during deposition, without rearrangement. Between $0.3T_m$ and $0.5T_m$ diffusion becomes important.

Hallam and Scrimshaw (1973 elaborate on this notion of rigidity as a barrier to solute diffusion. These authors list actual temperatures at which diffusion effects become important (T_d) for several common matrix gases. While the values of T_d for N_2 and O_2 are 30K and 26K (approximately one half of the normal melting points of 63.2K and 54.4K, respectively), it was found that CO_2 is an exception. For CO_2, T_d = 63K, while T_m =

216.6K. Thus for CO_2, the T_d/T_m = 0.29. This T_d value (63K) corresponds well with the minor desorption peak at 63K for CO_2- isolated NO given in Figure (3-5).

Guillory and Hunter (1969) employed IR spectroscopy in a study of the dimerization and aggregation of NO in N_2 matrices. With matrix ratios of 500:1 (N_2:NO) and deposition onto a 4K cryosurface, complete isolation of NO resulted; i.e., no dimer or higher aggregate bands were observed spectroscopically. Heating the cryofrost to 15K and rapidly recooling to 4K brought about limited dimerization. Heating to 40K and then recooling to 4K resulted in an IR spectrum identical to that of bulk NO. Thus, starting with a very dilute matrix and heating it to 10K above its T_d value, total aggregation of the solute NO, as measured by IR absorption, occurred. It must be noted here that Guillory and Hunter (1969) found CO_2 too rigid for their experiments, though they were interested in the 15K to 40K temperature range, where the CO_2 matrix would be highly rigid.

Smith and Guillory (1977, 1977A) investigated NO isolated in O_2 at O_2:NO ratios of 100 to 300:1 on a CsI window initially at 13K. They found that NO deposited in this manner yielded IR spectra indicative of complete isolation. However, by heating the matrix to 35K in a six second interval and then recooling to 13K, limited migration was induced. In this experiment, IR analysis revealed NO dimer formation, as well as products of NO oxidation. Cis-$(NO)_2$ was found to be the most stable dimer. Thus again in this case, rapid dimerization (and reaction) occurred when the isolated matrix containing NO was heated to 9K above its

diffusion temperature (T_d).

The most realistic conceptualization of the cryofrost structure would be the microcrystalline state (Cradock and Hinchcliffe, 1975); i.e., small crystals surrounded by regions unoriented with respect to each other. Multilayer deposits of O_2 and Xe, grown by Horl and Suddeth (1961), and studies by electron diffraction, reveal a crystallite size of approximately 100Å. Venables and Ball (1971) grew rare gas crystals in the 40K to 50K temperature range, and found grain sizes of $\leq$2000Å by electron microscopy. Thus crystallite sizes should range from 100Å to 1000Å in radius, on the average.

As in the work of Chadwick and Glyde (1977), a mean penetration depth (MPD) can be defined as

$$MPD = (Dt)^{0.5}$$

where D is the diffusion rate and t a characteristic time. Estimating the average radii of the crystallites obtained by deposition as 500Å and the characteristic time as 100 seconds, (a conservative estimate of the time available for diffusion), a diffusion rate of approximately 2.5×10^{-13} cm^2/s would be necessary for the MPD to be equal to the crystallite radius; i.e., at this diffusion rate, much of the trapped NO would be able to migrate to the grain boundaries.

Although diffusion rate expressions were not found in the literature for the NO-CO_2 system, examination of a different system should allow an order-of-magnitude estimate for the possible diffusion rates. Self-diffusion in Kr, which

has a T_d of 50K (Hallam and Scrimshaw, 1973) has been shown to be well represented by

$$D = 5 \exp(-4800/\underline{R}T),$$

where D is the diffusivity in cm^2/s, $\underline{R}$ is the gas constant, and T is the temperature in K (Chadwick and Morrison, 1970). At 80K, this expression yields a diffusion rate of 3.8×10^{-13} cm^2/s, which is of the correct order of magnitude for the mean penetration depth desired. Thus in this rare gas solid, the order of magnitude of the diffusion coefficient is high enough to allow diffusion to the grain boundaries.

Parker et al. (1969) reported that the activation energy for diffusion along grain boundaries is approximately half of its value for crystalline lattices. Thus grain boundary diffusion coefficients are approximately 10^6 times larger than those for lattices, making lattice diffusion the only effective barrier. In this work on self-diffusion in Ar, it was assumed that the concentration of isotopic Ar in the grain boundaries is equal to that in the vapor during the experiment; i.e., there is no effective barrier to diffusion along the grain boundaries.

Meyer (1971), in a general review of diffusion in cryofrosts, noted that diffusivity should be dependent on relative solute-solvent molecular size. Thus a small solute in a larger solvent matrix, such as NO in CO_2 in the current work, should exhibit a larger diffusion coefficient than in self-diffusion, for example. Thus, the estimate of Kr self-diffusion rates at 80K may actually underestimate that for the NO-CO_2

system, with the NO diffusion coefficient being significantly greater, thereby allowing even greater mobility during desorption, which again leads to aggregate formation and ultimately, disproportionation.

Thus it is reasonable to assume that during heating of the NO-CO_2 matrix, diffusion of NO can occur readily prior to CO_2 desorption, and that during this process NO diffuses to the crystalline grain boundaries, where it meets with little diffusional resistance, leading to agglomeration which provides the necessary four-body sites for the disproportionation reaction. From the experimental evidence, it is likely that the actual disproportionation reaction occurs during the desorption process. Predicting a mechanism for this reaction would be sheer speculation without the aid of further analysis using surface analysis techniques, such as IR spectrophotometry.

It is interesting to note that in Figure (3-5), a NO desorption peak does occur at 64K, but is only approximately 2.4% of the main peak at 88K. It is possible that this minor peak represents that portion of the NO deposited that phase-separates upon deposition, or perhaps that originally resided in the grain boundaries, while the majority of the NO deposited is still locked in the CO_2 matrix and thus cannot desorb until agglomeration and disproportionation occur.

3.1-3. Ozone Recombination

In view of the preceeding on NO disproportionation, it is evident that reactions can occur at cryogenic temperatures. Thus, studies were conducted to determine whether or not O_3 recombines during the deposition and desorption process. With a normal boiling point of 161.9K in comparison to 90.2K for oxygen (Dean, 1973), O_3 has a significantly lower vapor pressure than O_2. Thus, even though O_3 does not exhibit a parent peak at mass 48, it is possible that O_3 deposited as a mixture in O_2 can survive the desorption of the more volatile O_2 and remain on the cryosurface, only to sublimate at a temperature at which its vapor pressure is close to the system pressure. By depositing such a mixture and following the oxygen parent peak during desorption by TPD, an "extra" desorption peak may occur at relatively high temperatures, corresponding to O_3.

In one experiment, 1.1×10^{-5} g mol of a mixture of 1.59% O_3 in O_2 were deposited on the gold-flashed, stainless steel surface and desorbed by the TPD method. Another companion run was a blank, in which 9.3×10^{-6} g mol of pure O_2 were deposited and desorbed in a similar fashion. The resultant TPD spectra are presented in Figure 3-6. These spectra show that there is no substantial difference in desorption patterns between ozonated and non-ozonated oxygen. An extra desorption peak due to O_3 occurring after the main O_2 desorption peaks would have been clearly visible. This implies that either O_3 desorbs with O_2, (i.e., it is carried over), or that it survives on the surface during the desorption

of O_2 but concentrates and decomposes immediately to form O_2. Since the product of the recombination, O_2, is indistinguishable from either the reactant (O_3) or the matrix (O_2) with this analytical technique, and the concentration of O_3 in O_2 in the feed stream has a maximum of 2.25%, it is evident that this technique cannot be employed satisfactorily to study O_3 regeneration.

Due to these findings, the following series of O_3 regeneration experiments utilized chemiluminescence as the O_3 detection technique, employing the titration method, as described in section 2.1-2. Thus a procedure was developed in which a known quantity of O_3 in O_2 at a known concentration was deposited on the 15K cryosurface, flash desorbed with N_2, and the resultant gas mixture analyzed for O_3 using chemiluminescence. The number of g mol of O_3 both deposited and recovered after desorption could be calculated, and this information employed to determine whether or not O_3 could be deposited and then desorbed in a quantitative manner.

In one experimental run, 3.17×10^{-4} g mol of approximately 1.6% O_3 in O_2 were deposited on the cryosurface and subsequently flash desorbed with N_2. By calculating the amount of O_3 deposited, it was determined that the resultant gas would have an O_3 concentration of 12.8 ppm if 100% of the deposited O_3 was recovered. Since a direct reading of the panel meter during chemiluminescence titration overestimates the concentration of O_3, as illustrated by the calibration curve of Figure (2-5), the uncorrected meter reading would be on the order of 98 ppm

with a raw sensitivity on the lowest scale of approximately 0.2 ppm. The result of the experiment was surprising in that the O_3 reading obtained upon desorption was zero, implying that all of the ozone deposited had recombined.

This lack of ozone recovery was not due to calibration errors. Since the ozone generator and chemiluminescence analyzer were calibrated while feeding the sample stream through the same valves, fittings, and tubing involved in feeding the sample gas to the cryosurface, any small O_3 loss in this system should have been compensated for. With an uncorrected panel meter reading of 98 ppm expected, with a sensitivity of 0.2 ppm, the ozone loss experienced, if due to a calibration error, would require an error on the order of a factor of 500; i.e., the deposit actually made had to be on the order of 1/500 of the amount calculated. Possible calibration errors include the vacuum system pumping speed, the ionization gauge corrections for the various gases, and the initial O_3 composition in the feed stream. The pumping speed, however, is conduction limited, and thus cannot change appreciably. The ion gauge response to N_2 as compared to the mass spectrometer readings was consistent, making error on its part unlikely. The ozone concentration in the feed stream was also shown to be reproducible by wet titration. Thus it was concluded that for an ozone loss this pronounced, O_3 must have decomposed during the desorption process, similar to NO disproportionation. Therefore, it was decided to increase the ozone concentration in the feed stream and the total deposit

amount, with the objective of ascertaining whether or not any O_3 could indeed be deposited and then recovered from the solid state.

The experimental runs listed in Table 3.1 were conducted by depositing 2.25% O_3 in O_2 and varying the deposit time, and thus the amount of mixture deposited, followed by flash desorption. Figure (3-7) displays the same information graphically. A linear fit of these data yields a slope of 0.6096, and ordinate intercept of -3.29×10^{-6}. There are several features of note in this figure. The abscissa intercept is at 5.4×10^{-6} g mol O_3. Thus it appears that below this amount of O_3 deposited, all of the O_3 decomposes, as above. It was shown previously, as in the case of NO in N_2, that if a matrix material is more volatile than the solute species, phase separation will occur; i.e., the matrix material will sublimate, leaving concentrated solute on the surface. Small amounts of O_3 concentrated in this manner seem to recombine completely. This is also supported by TPD results where 1.7×10^{-7} g mol of O_3 were deposited, and the desorption spectra revealed no distinctive desorption peaks at high temperatures (>45K). It is possible that O_3 separates from the O_2 matrix in this manner, recombines immediately and desorbs at the tail-end of the desorption spectrum.

The line drawn in Figure (3-7) also has a slope of approximately 0.61, implying that although ozone is recovered at higher absolute quantities deposited, the relationship is still not one to one; i.e., a percentage of the ozone deposited

in the quantity over that necessary to overcome the initial disappearance, is also converted. Figure (3-8) is a plot of percent conversion of O_3 to O_2 (moles deposited-moles recovered)/ moles deposited) versus the number of moles of O_3 in the deposit. Note that conversion decreases with increasing deposit layer amount, which may imply that competition for a limited number of catalytic sites may be occurring. Conversion seems to level off at approximately 55% at higher deposits, which may reflect the fact that thicker deposits effectively enjoy a longer residence time on the surface. Catalytic limitations and variations in reaction time may compensate, yielding a near constant percentage conversion at the higher deposit thickness.

An estimate of the heat of reaction for decomposition at 50K in the solid phase shows it to be exothermic, with ΔH_R= -69.5 kcal/g mol, calculated from data given by Reid et al. (1977) ($C_p(T)$) and Dean (1973) (heats of formation, fusion, and vaporization). This reaction is therefore thermodynamically favorable, and thermal chain reactions are again possible. As for the previous experiments, it appears that O_3 decomposition may also be self-catalytic.

In another series of experiments, annealing the O_3 in O_2 matrix was attempted a la Smith and Guillory (1977), in an effort to determine if increased aggregation induced by this process would increase the conversion of O_3 to O_2. 2.3×10^{-5} g mol of O_3 were deposited at 15K (2.25% O_3 in O_2), and then

annealed to 35K, recooled to 15K and held at 15K for 5 minutes. Flash desorption yielded 6.6×10^{-6} g mol of O_3 recovered in the resultant gas, as compared to an estimated value of 1.07×10^{-5} g mol, or a factor of 1.6 greater than the amount of O_3 recovered experimentally. Thus it seems that annealing does have some affect in increasing decomposition of ozone. The data for these two experiments are shown in Figure (3-9, curve B). Curve A of this figure is the data of Figure (3-7). There is a substantial difference between these data sets.

In order to attempt to prove conclusively that annealing was in fact responsible for reduction of O_3 recovery, two experiments were performed, depositing 4.39×10^{-5} and 3.4×10^{-5} g mol of O_3, respectively, in an O_2 matrix at a concentration of 2.25%. Flash desorption and subsequent analysis yielded 1.58×10^{-5} and 1.04×10^{-5} g mol of O_3 recovered. These data are presented in Table (3.2), along with the previous data. These points are also shown in Figure (3-9) as part of curve B. It is noted that the experiments performed with and without annealing fall on the same straight line, with a least squares slope of 0.44, on ordinate intercept of -3.79×10^{-6} and correlation coefficient of 0.99. Thus annealing cannot be the cause of the increased decomposition of O_3 which occurred for this experimental set.

These results can be explained in terms of surface aging with a concommitant increase in catalytic activity with respect to O_3 decomposition. Although gold should be catalytically inert, the original

gold flashing may not have been complete, leaving parts of the underlying surface exposed and subject to thermal cycling and exposure to concentrated oxidants, which might have caused chemical transformations. The experiments listed in Tables (3.1) and (3.2) were run approximately 2 to 3 weeks apart, with many other experiments occurring in between.

The work of Jenkins (1959) dealing with high concentration liquid ozone handling techniques reports that hydrocarbons, as well as other contaminants, are thought responsible for initiating O_3 recombination in liquid ozone. Arlin and Warneck (1972) investigated gas phase O_3 decomposition and tested CO as an initiator of a thermal chain reaction, resulting in the decomposition of O_3 by O_3-O_3 recombination. These authors found that rapid reaction occurred when CO and O_3 were mixed, but after further testing included that a low level contaminant in the CO was actually the chain initiator. Since CO is one of the major background species in oil diffusion-pumped vacuum systems, it was decided to test CO as a decomposition initiator by using it as a base sublayer for the O_3-O_2 mixture deposition and subsequent flash desorption.

In one experiment, 1.9×10^{-4} g mol of CO were deposited on the 15K gold-flashed surface, followed by 2.1×10^{-5} g mol of O_3 in a 2.25% O_3-O_2 mixture. Upon flash desorption, approximately 1.1×10^{-6} g mol of O_3 were recovered, an amount substantially less than would be expected from the previous experiments (Figure (3-9) curve B). The experiment was repeated with a

larger deposit of $4.x\ 10^{-4}$ g mol of CO, followed by 5.76×10^{-5} g mol of O_3 deposited in a 2.25% mixture with O_2. This experiment resulted in 1.1×10^{-5} g mol of O_3 being recovered, again a decrease with respect to the amount expected as given by Figure (3-8), curve B. Thus the preliminary results suggested a significant increase in O_3 decomposition can be induced by depositing CO on the cryosurface as a base layer.

In order to confirm this result, experimental blank runs were performed without CO deposition. For these runs 2.5×10^{-5} and 3.7×10^{-5} g mol of O_3 in a 2.25% mix with O_2 were deposited, respectively, and 3.42×10^{-6} and 3.08×10^{-6} g mol of O_3 were recovered. These results are listed in Table (3.3), and presented in Figure (3-8), curve C. They show that although there again was a significant decrease in the amount of O_3 recovered, the effect was independent of the CO deposit sublayer. The slope of the straight line drawn through the data of Figure (3-8), curve C is 0.25, and its ordinate intercept is -4.03×10^{-6}, quantifying the difference between these data and that of curves A and B. It should be noted here that the data of curve C were taken approximately 4 months after the initial runs represented by curve B of Figure (3-9).

Thus, over a period of five months, it was found that ozone decomposition on the same cryosurface increased significantly, yielding a linear relationship within any single set of experiments, but with constantly decreasing slope between experimental sets (Figure (3-9). Calibration drifts cannot

account for this behavior. The most likely changes in calibration would occur in either the ozone generator or the chemiluminescence analyzer. In order to determine if this was the case, the 5.6 ppm calibration standard was introduced to the reaction chamber of the chemiluminescence analyzer, and the panel meter read 5.6 ppm, proving that a drift in the analyzer calibration was not at fault. The ozone generator was then recalibrated by the wet titration procedure, described previously, and the calibration curve was found to be reproducible to within 7% of the original calibration. Thus, it is not likely that an experimental calibration shift in the ozone generator was responsible. Therefore, it appears that the condition of the cryosurface is the most likely factor which could account for the significant change in decomposition behavior. A review of the known literature on this subject follows.

3.1-4 Ozone Recombination Literature

The early work of Platz and Hersh (1956) and Jenkins (1959) on producing and purifying pure liquid O_3 are replete with reports of explosions; i.e., rapid decomposition of O_3 to O_2 with the subsequent stoichiometric increase in volume and thermal energy. It was believed at the time that the principal sensitizers for the decomposition reaction were organic contaminants, and that liquid ozone was only stable when the level of sensitizers was restricted to below 20 ppm. Since the decomposition is exothermic, it was believed that a thermal chain occurred; i.e., the reaction provides energy necessary for neigh-

boring molecules to react. It was also noted that explosions usually occurred during a phase change (usually boiling or vacuum evaporation).

Ardon (1965) noted that liquid O_3 is highly explosive, and is sensitized by small amounts of hydrocarbons as well as species such as H_2. He also reported that some metals, particularly in the Fe and Pt groups, metal oxides, peroxides and hydroxides are active O_3 decomposition catalysts.

Relevant work on this type of experimental system has been performed and reported by Emel'yanova et al. (1964, 1964A). This work deals with the catalytic decomposition of liquid O_3 at cryogenic (77K and 99K) temperatures. It was found that Pt and Pd catalysts were highly active in this regard, and it was implied that the conversion was nearly complete. Fe_2O_3 and NiO were found to be relatively inert, although they have been reported as active in gas phase decomposition. The authors postulated a mechanism by which the activation energy for the liquid phase reaction was supplied by the exothermic decomposition of neighboring O_3 molecules. It was also found that dilution of O_3 with liquid N_2 or O_2 had no influence on the decomposition rate, which implies that the surface reaction was the rate-determining step.

The catalytic activities of NiO (Houzelot and Villermaux, 1976) and Fe_2O_3 (Neely et al., 1975) towards decomposition of O_3 in the gas phase are well known. In fact, Fe_2O_3 (Neely et al., 1975) is so effective, that a room temperature stream of 2 to 3% O_3 in O_2 was found to decompose to the extent that

no ozone was detectable, at a sensitivity of 10^{-8} parts of ozone to oxygen in the exit stream, when the sample was run through a packed bed of Fe_2O_3 mesh. Thus, Fe_2O_3 and NiO were found to be active in the gas phase, but relatively inactive in the bulk liquid phase. This suggests that these two metal oxides may be orientationally hindered from acting as catalysis in the bulk liquid phase by electrical double layer constraints (Marron and Prutton, 1965), an effect which should not prevail in very thin films of cryofrost, the orientation of which is determined by different factors.

Thus, catalytic activity of NiO and Fe_2O_3 on the base stainless steel in the cryofrost experiments may be responsible for the observed behavior. It is entirely possible that the gold-flashing on the stainless steel disk was not completely successful in covering the stainless steel surface. This in turn allowed slow oxidation of the surface from repeated exposure to concentrated oxidants and repeated rapid thermal cycling. Stainless steel is an alloy of Fe, Ni, Cr, and other elements, and thus oxidation of the surface layer would probably yield Fe_2O_3 and NiO. With the absence of a significant double layer effect, as might occur for liquid O_3, and for very low absolute deposit quantities, catalytic activity of this surface is possible. Thus, it is hypothesized that repeated O_3 deposition and desorption on the gold-flashed surface increased its catalytic activity towards O_3 recombination by increasing the surface concentration of NiO and Fe_2O_3, formed by oxidation of the exposed stainless steel with concentrated O_3, a resultant of phase separation of O_2 from the O_2-O_3 mixture. This

hypothesis is supported by the apparent increasing catalytic activity illustrated by the three curves in Figure (3-9). In addition, visual inspection of the surface revealed that the gold-flashed cryosurface had lost much of its original luster in areas of high condensate loading.

The question of whether or not the decomposition of O_3 on the surface is initiated by the exothermic reaction of O_3 with some low level contaminant species yet remains. The primary identifiable contaminant species in the current system are H_2O and CO. The oxidation of CO with ozone has been considered as a possible atmospheric reaction, and has, as mentioned previously, been studied by Arin and Warneck (1972). These investigators studied this reaction on a laboratory scale, and found that that the initial mixing of O_3 and CO in the gas phase at low pressures produced an immediate intense reaction. Strangely enough, however, they found that the reaction proceeded almost to completion and then abruptly stopped, with little additional conversion occurring subsequently. This led the authors to hypothesize that either the products formed, (CO_2 and O_2) were inhibitors of the reaction, or that an impurity in one or more of the feed streams was acting as an initiator. By dilution studies, they were able to prove that the gaseous products were not inhibitors, thereby leaving the second possibility open. In this regard they noted that if an excess of CO was employed and the reaction allowed to exhaust the initial O_3 added, and the excess CO was separated from the reaction products

by adsorption on charcoal, the CO thus recovered would not react with ozone significantly. Therefore, the authors claimed that the initiator was a contaminant in the CO feed gas, even though the CO had been carefully prepurified. The possible contaminant remained unidentified. This example illustrates that low levels of unidentified contaminants which exist in the background of the vacuum chamber, as a result of introduction in the feed gas or cracking of vacuum pump oil, may indeed initiate ozone decomposition on the cryosurface.

Thus it has been found that the differences in curves A, B, and C of Figure (3-9) may be due to oxidation of the exposed portion of the gold-flashed surface to Fe_2O_3 and NiO, which have been shown to be gas phase O_3 decomposition catalysts. This does not exclude the possibility that the reaction is initiated by a volatile impurity in the background or O_3 feed itself, but it does cast doubts on the effectiveness of CO as the initiator, an effect which has been confirmed experimentally here.

3.1-5. NO Oxidation

Flash desorption (with pure nitrogen) of a 1/1/44.4 mixture of $NO/O_3/O_2$ (i.e., 4.6×10^{-5} g mol NO, 4.6×10^{-5} g mol O_3, and 2.0×10^{-3} g mol O_2) from the gold-flashed stainless steel cryosurface (maintained at 15 K during deposition of the mixture), followed by chemiluminescence analysis, yielded $NO/NO_x = 0.224$. This value is significantly less than those found for self-disproportionation of pure NO, thereby indicating additional conversion of NO to NO_2. Due to the relatively large

amount of oxygen present, however, the fraction of this additional conversion attributable to oxidation by ozone vs. oxygen could not be immediately discerned. In order to examine this question further, blank experiments (i.e., with no ozone) were conducted. In one such experiment a 1/44.4 mixture of NO/O_2 was deposited on the 15 K gold-flashed cryosurface and flash desorbed with pure nitrogen. Chemiluminescence analysis of the resultant mixture yielded $NO/NO_x = 0.48$, which is well within the range of the pure NO self-disproportionation results reported previously. Thus, molecular oxygen clearly has a minimal effect on NO conversion, if indeed any at all, and the enhanced oxidation observed for ozone-containing mixtures is attributable to ozone. The reaction:

$$NO + O_3 \longrightarrow NO_2 + O_2 \qquad (R5)$$

is, of course, also exothermic ($\Delta H_r = -48$ kcal/g mol at 83 K in the solid phase, estimated from data given by Reid et. al., 1977, and Dean, 1973). Therefore an autothermal chain reaction mechanism is also possible, just as for NO self-disproportionation and ozone recombination.

The data of Honig and Hook (1960) show that under our experimental conditions the vapor pressure of NO is less than O_2, thereby allowing the formation of a concentrated $NO\text{-}O_3$ mixture upon initial desorption of O_2. This fact could also account for the minimal effect of O_2 on NO conversion; i.e., the bulk of the O_2 may desorb prior to the NO becoming reactive enough for significant conversion to occur.

More quantitative conclusions than included in the preceeding are currently not possible due to the complex nature of the detailed reaction mechanism of NO/O_3 mixtures. It is noted that in addition to direct oxidation of NO by ozone (R5), the competitive processes of NO self-disproportimation (R3)and ozone recombination occur as well.

The only work we are aware of which is even somewhat relevant to the preceeding results is that of Lucas (1977) and Lucas and Pimentel (1979). In this work the reaction (R5) was studied in the solid phase (not upon thermal desorption) by IR spectrophotometry. Typically cryofrosts of compositions such as $NO/O_3/N_2$ = 1/30/250 were deposited on a 12 K CsI window and the growth of the 1617 cm^{-1} band with time was attributed to the production of NO_2. Even though this product was clearly evident, the high dilution ratios employed resulted in barely discernible changes in the reactant concentrations. The $NO-O_3$ complex was hypothesized as the reaction intermediate, and the reaction rate data were found to be first order with respect to the concentration of the complex, with a preexponential factor of 1.45×10^{-5} s^{-1} and an activation energy of 106 cal/g mol in the solid phase at 12 K. This activation energy is of the order required for orientation rearrangement in rare gas matrices, and more than an order of magnitude less than the 2.3 kcal/g mol reported for the gas phase version of reaction (R5). It was therefore hypothesized that matrix rearrangement could be the rate-limiting step.

Clearly, the experimental conditions and conversion levels of Lucas (1977) are quite different than our own, but the mechanism involving the $NO-O_3$ complex may be similar to that which occurs upon warming the frost to desorption in our experiments. For a similar activation energy on the order of that required for matrix rearrangement, raising the temperature would accelerate reorientation, as well as increase the number of potential $NO-O_3$ reaction pairs by increasing diffusivities. The simultaneous effect of both mechanisms could increase the overall reaction rate considerably over that observed by Lucas (1977).

3.2 IR Spectrophotometry

3.2-1. N_2O

N_2O was deposited on the CdTe sample window as follows: With the refrigerator off and the system warm, the double pattern fine metering valve was set such that the background pressure rose to a steady-state value of 50 mtorr, with an upstream delivery pressure of 2.5 psig. The micrometer settings for this flow rate were recorded. The metering valve was then closed and the system allowed to return to its base pressure (<1 mtorr). The refrigerator was then turned on and the sample holder/window assembly cooled to 18 K. With the system completely cold, the metering valve was reset to the original flow rate determined above. N_2O was allowed to flow into the system at this rate for one minute. No increase in the background from the $\sim$1 mtorr level was detectable, thereby implying that the bulk of the

N_2O admitted was collected mainly on the sample window and holder.

A series of IR spectra of the condensate were recorded as a function of window temperature. One such representative spectrum is presented in Figure (3-10). The fundamental modes of N_2O in the condensed state are clearly evident; i.e., the stretching modes, ν_3 and ν_1, at 2240 cm^{-1} and 1290 cm^{-1}, respectively, and the bending mode, ν_2, at 595 cm^{-1} (Hallam, 1973). Some of the other features are most probably combinations and overtones of the fundamentals.

A spectrum of the same sample, taken one hour later is presented in Figure (3-11). In this figure it is quite evident that all the features remained the same as in Figure (3-10) except for the broad absorption centered about 3200 cm^{-1}. This feature clearly grew in magnitude over the one hour period. This absorption continued to increase over time even during heating of the N_2O sample to desorption as shown in the composite presented in Figure (3-12). The N_2O sample disappeared at $\sim$100K with no obvious changes in the N_2O features between 17K and 100K. But the 3200 cm^{-1} absorption continued to grow to $\sim$200K where it abruptly disappeared entirely.

A typical background spectrum of the sample window cold (17K) with no condensed gas sample is presented in Figure (3-13) for comparison. The features at 2700 cm^{-1} and 1080 cm^{-1} are always present in all spectra (e.g., at atmospheric pressure and under vacuum, with and without windows, with and without condensed sample, etc.) and are, therefore, attributed to the

instrument. However, the 3200 cm^{-1} absorption is also present and behaves in the same manner as in the N_2O condensed sample spectra; i.e., it steadily increases with time. Thus, this feature is definitely not due to N_2O, but is indicative of additional accumulation of the species responsible over the time span of the experiments as a result of continual deposition from the gas phase and/or from processes occurring in the condensate. It is believed that the 3200 cm^{-1} absorption is due to water accumulating and polymerizing on the sample window from the background in the vacuum chamber. This frequency has been observed for hydrogen bonded species with OH groups in polymerized form in condensed phases (e.g., see Bellamy, 1975). In addition, the temperature of disappearance for this feature (∿200K) is indicative of water condensate desorption under vacuum (e.g., see Calo et. al., 1981).

3.6-2. CCl_2F_2 (Freon 12)

CCl_2F_2 was deposited on the CdTe sample window in exactly the same fashion as N_2O. However, due to the much stronger absorptions exhibited by this species, a smaller sample was used; i.e., 15 s deposition time instead of one minute as for N_2O. A typical spectrum is presented in Figure (3-14). The spectrum in the vicinity of the major absorption features is repeated and superimposed under different operating conditions (see figure caption) to show these more clearly. The symmetric and asymmetric C-F stretching modes at 1155 and 1095 cm^{-1} and the corresponding C-Cl modes at 910 and 870 cm^{-1}

are clearly evident. The principal features of the spectrum seemed to remain constant as the sample was warmed. The visible condensate and absorption vanished over the temperature range ∿100-110K. This range agrees quite well with CCl_2F_2 temperature programmed desorption spectra (Calo et. al., 1981).

4. Future Work Plans

The preceeding results clearly demonstrate the capability of the cryogenic IR cell to enable the detection of species behavior in the condensed state at low temperatures. During the term of the successor contract (F19628-81-C-0157) at Brown University, the IR spectrophotometry apparatus will be applied to the investigation of the conversion of NO to NO_2 in the condensed state, both due to self-disproportionation, and oxidation by ozone and oxygen. This data will be used to establish the mechanisms involved in NO conversion as a function of rate of deposition (i.e., matrix morphology), temperature, and composition. The kinetics of these reactions in the condensed state at low temperatures will be useful for assessing the impact of these reactions on NO/NO_2 ratios obtained from stratospheric whole air samples. Since the NO dimer has been postulated as an intermediate in the oxidation of NO by oxygen mechanism in the solid state, this work should naturally lead to the study of molecular complex formation and aggregation of other stratospheric species of interest in different cryofrost matrices. In addition, the apparatus will also be adapted to begin the radical species studies.

REFERENCES

Abe, H., Schultze, W., Chem. Phys. 41, 257-63, 1979

Addison, W. E., Barrer, R. M., J. Chem. Soc. Lond. 757-69, 1955

Ardon, M., Oxygen-Elementary Forms and Hydrogen Peroxide, W. A. Benjamin, N. Y., 1965, p58-67

Arin, L. M., Warneck, P., J. Phys. Chem. 76, 1514-16, 1972

Bellamy, L. J., The Infra-red Spectra of Complex Molecules, Wiley, N. Y., 1975.

Calo, J. M., R. J. Fezza, and E. J. Dineen, "Gas-Surface Interactions in Cryogenic Whole Air Sampling", AFGL-TR-81-0162, Air Force Geophyics Laboratory, Hanscom AFB, MA.

Chadwick, A. V., Glyde, H. R., Rare Gas Solids, Vol. 2, Klein, M. L., Venables, J. A., eds, Academic Press, N. Y., 1977, p1152-1252

Chadwick, A. V., Morrison, J. A., Phy. Rev. B 1, 2748, 1970

Cradock, S., Hinchcliffe, A. J., Matrix Isolation, A Technique For the Study of Reactive Inorganic Species, Cambridge Univ. Press, London, 1975

Dean, J. A., ed., Langes Handbook of Chemistry, McGraw-Hill, N. Y., 1973

Deitz, V. R., Bitner, J. L., Carbon 11, 393-401, 1973

Emel'yanova, G.I., Lebedev, V. P., Kobozev, N. I., Chem. Abs. 60:9957e, 1964

Emel'yanova, G. I., Lebedev, V. P., Kobozev, N. I., Zh. Fiz. Khim. 38, 170-5, 1964 (A), Chem. Abs. 60:11412b, 1964

Guillory, W. A., Hunter, C. E., J. Chem. Phys. 50, 3516-23, 1969

Hallam, H. E., Scrimshaw, G. F., Vibrational Spectroscopy of Trapped Species, Hallam, H. E., ed., Wiley, N. Y., 1973, p12-66

Honig, R. E., Hook, H. O., RCA Reviews 21, 360,1960

Horl, E. M., Suddeth, J. A., J. Appl. Phys. 32, 2521-25, 1961

Houzelot, J. L., Villermaux, J., J. Chem. Phys. Phys-Chem. Biol., 73, 7-8, 1976, Chem. Abs. 86:22313g, 1976

Jenkins, A. C., Ozone Chemistry and Technology, Adv. In Chem. Series, A. C. S., Wash., D. C., 1959, p13-21

Lucas, D.,"Fast Reactions, Free Radicals, and Molecular Complexes Studies By The Matrix Isolation Technique," PhD Thesis, Univ. of Calif., Berkley, 1977, Univ. Micro. 77-31, 448

Lucas, D., Pimentel, G. C., J. Phys. Chem. 83, 2311-16, 1979

Lunsford, J. H., J. Phys. Chem. 74, 1518-1522, 1970

Marron, S. H., Prutton, C. F., Principles of Physical Chemistry, MacMillan, London, 1965, p847-849

Meyer, B., Low Temperature Spectroscopy, American Elsevier, N. Y., 1971

Neely, W. C., West, A. D., Hall, T.D., J. Phys. E 8, 543, 1975

Parker, E.H.C., Glyde, H. R., Smith, B. L., J. Phys. E 2, 691-5, 1969

Pimentel, G. C., Vibrational Spectroscopy-Modern Trends, Barnes, A. J., Orville-Thomas, W. J., eds., Elsevier Scientific, N. Y., 1977, p79-82

Platz, G. M., Hersh, C. K., Ind. and Eng. Chem. 48, 742-44, 1956

Redhead, P. A., Hobson, J. P., Kornelsen, E. V., The Physical Basis of the Ultrahigh Vacuum, Chapman and Hall, London, 1968

Reid, R. C., Prausnitz, J. M., Sherwood, T. K., The Properties of Gases and Liquids, McGraw Hill, N. Y., 1977

Smith, G. R., Guillory, W. A., Int. J. Chem. Kinetics 9, 953-68, 1977

Smith, G. R., Guillory, W. A., J. Mol. Spect. 68, 223-35, 1977 (A)

Varetti, E. L., Pimentel, G. C., J. Chem. Phys. 55, 3813-21, 1971

Venables, J. A., Ball, D. J., Proc. Roy. Soc. Lond. A 322, 331-54, 1971

TABLE (3-1)

INITIAL OZONE DECOMPOSITION EXPERIMENTS

Date	Run	Deposit (g moles O_3)	Recover (g moles O_3)	Initial Concentration (%)
7/10/80	239	5.05×10^{-6}	0	1.59
8/19/80	262	2.14×10^{-5}	8.49×10^{-6}	2.25
8/20/80	263	1.81×10^{-5}	8.84×10^{-6}	2.25
8/21/80	264	1.24×10^{-5}	4.26×10^{-6}	2.25
8/22/80	265	2.19×10^{-5}	1.05×10^{-5}	2.25
8.26/80	266	7.93×10^{-6}	1.30×10^{-6}	2.25

TABLE (3-2)

OZONE DESORPTION EXPERIMENTS

Date	Run	Deposit (g moles O_3)	Recover (g moles O_3)	Initial Concentration (%)
9/11/80	273	5.00×10^{-5}	1.32×10^{-5}	2.25
9/12/80	274	2.29×10^{-5}	6.62×10^{-6}	2.25
9/16/80	275	4.39×10^{-5}	1.58×10^{-5}	2.25
9/17/80	276	3.40×10^{-5}	1.04×10^{-5}	2.25

TABLE (3-3)

OZONE DESORPTION EXPERIMENTS

Date	Run	Deposit (g moles O_3)	Recover (g moles O_3)	Initial Concentration (%)
1/14/81	290	2.14×10^{-5}	1.08×10^{-6}	2.25
1/16/81	291	5.76×10^{-5}	1.08×10^{-5}	2.25
1/19/81	292	2.47×10^{-5}	3.42×10^{-6}	2.25
1/23/81	293	3.66×10^{-5}	3.08×10^{-6}	2.25

Figure (3-1) Thermal desorption spectrum of mass peak m/e = 28 following deposition of pure NO.

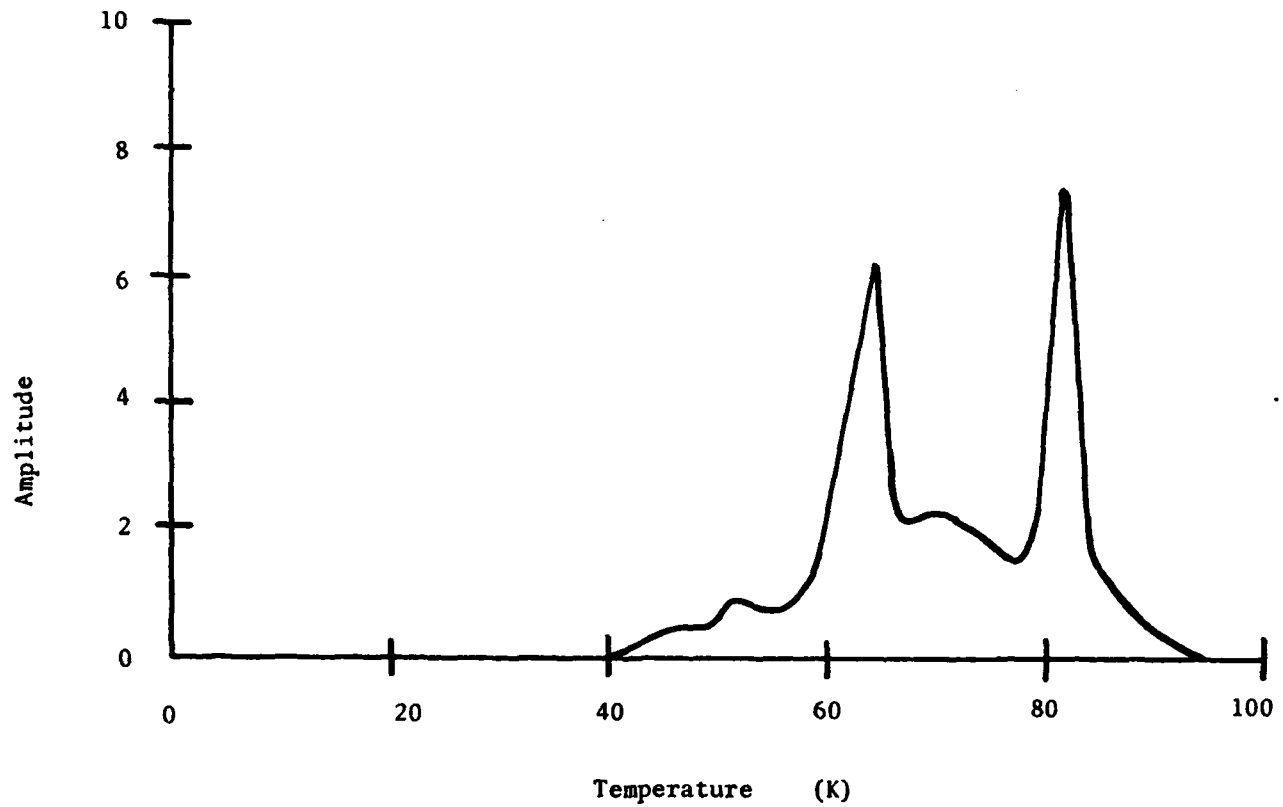

Figure (3-2) Thermal desorption spectra for mass peaks m/e = 28 and 30 following deposition of pure NO.

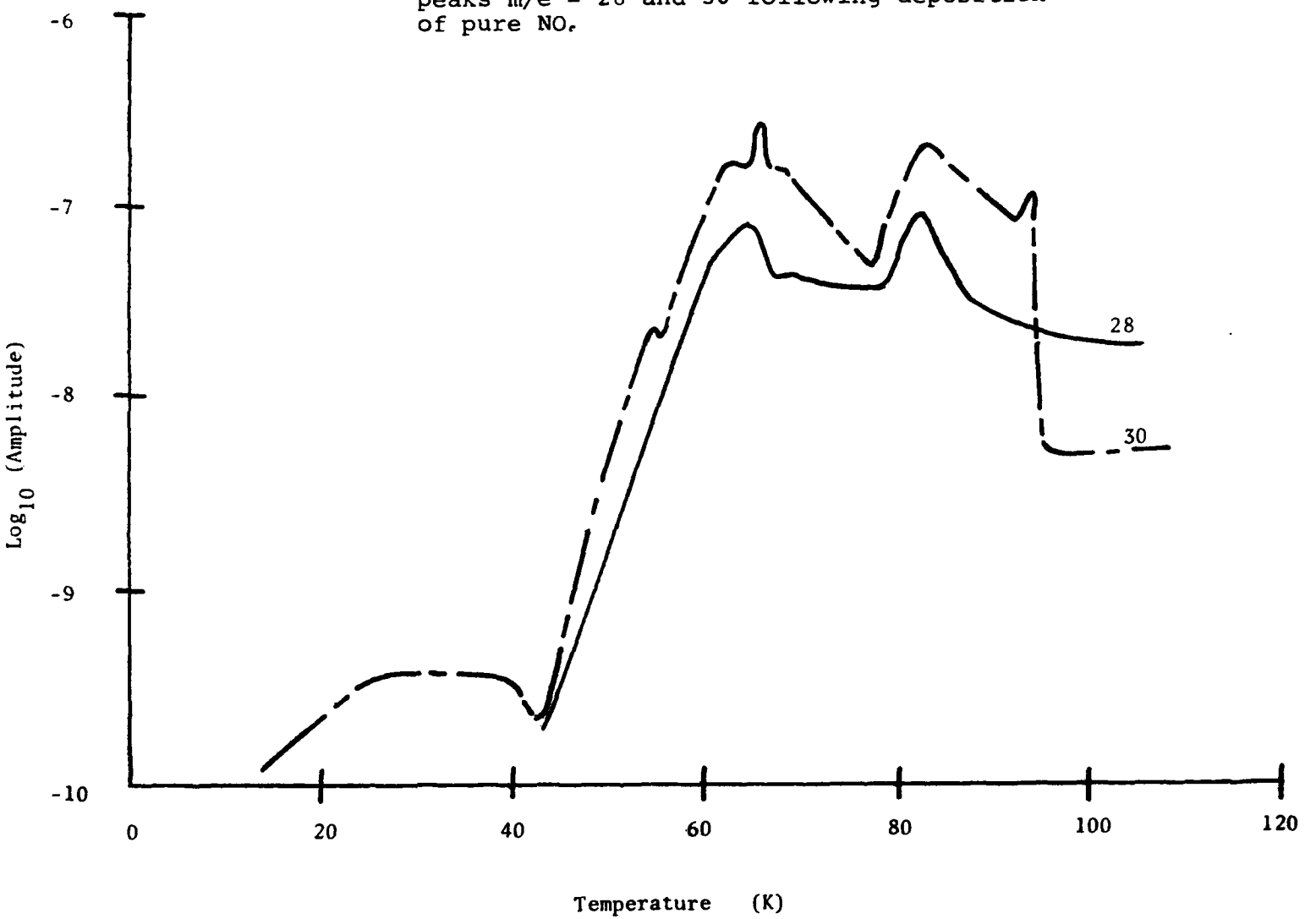

Figure (3-3) Thermal desorption spectra for mass peak m/e = 28: (A) Following deposition of 5% NO in N_2; and (B) Background.

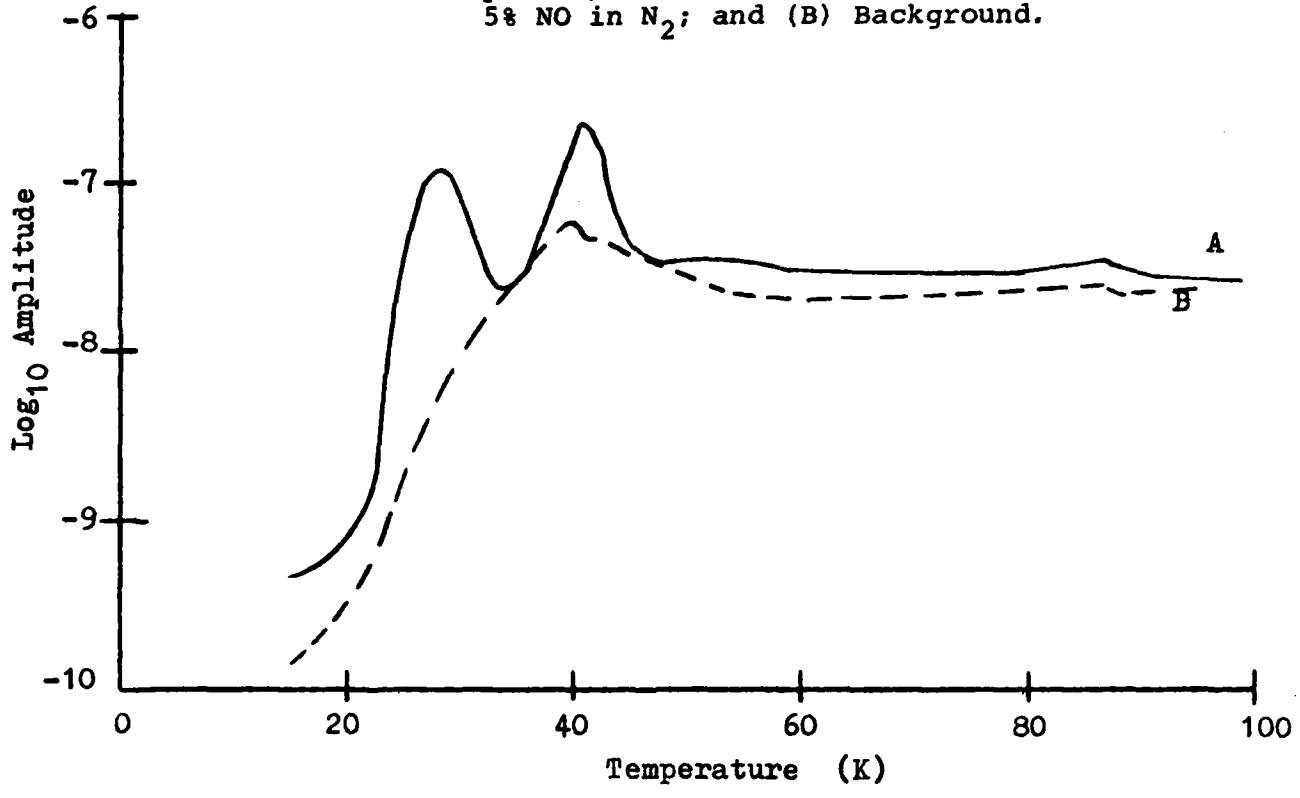

Figure (3-4) Thermal desorption spectrum of mass peak m/e = 30 following deposition of 5% NO in N_2.

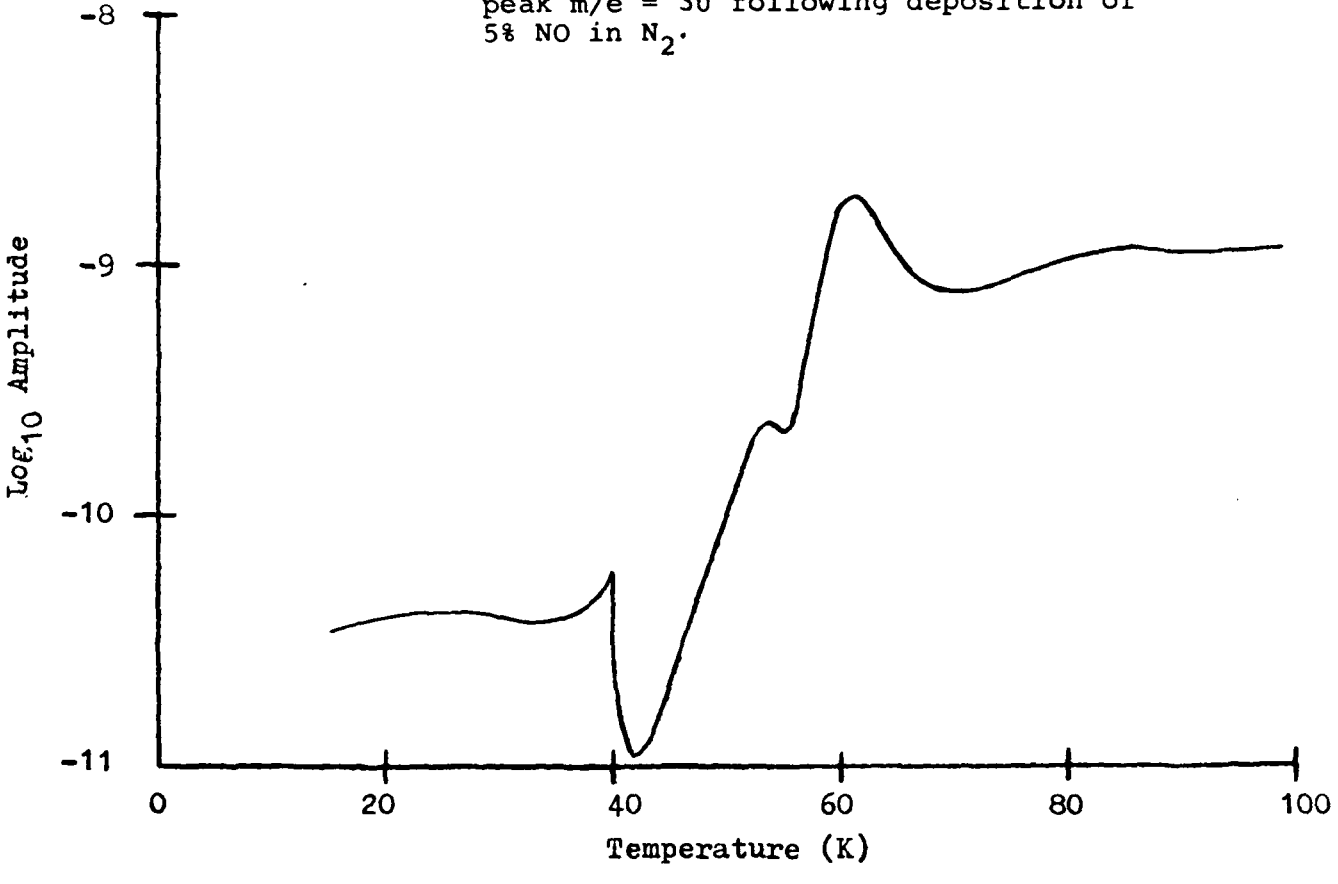

Figure (3-5) Desorption Spectra of NO In A NO-CO_2 Mixture (A), CO_2 In A NO-CO_2 Mixture (B), And Pure CO_2 (C).

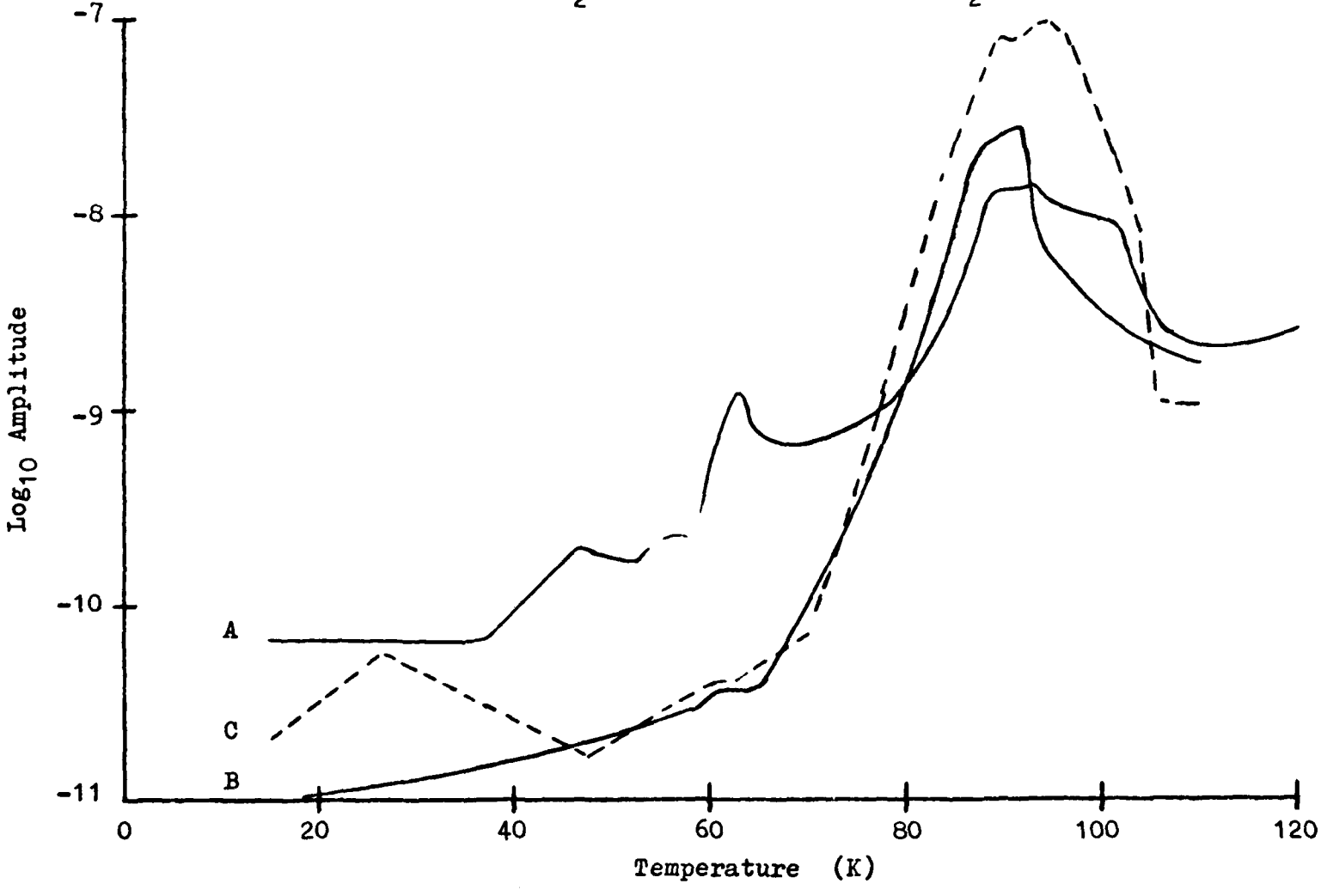

AD-A114 661 PRINCETON UNIV NJ DEPT OF CHEMICAL ENGINEERING F/G 9/1
CHEMICAL REACTIONS AND MOLECULAR AGGREGATION IN CRYOGENIC WHOLE--ETC(U)
JAN 82 J M CALO, R J FEZZA, G F RYAN F19628-80-C-0066
UNCLASSIFIED AFGL-TR-82-0061 NL

END
DATE FILMED
6 82
DTIC

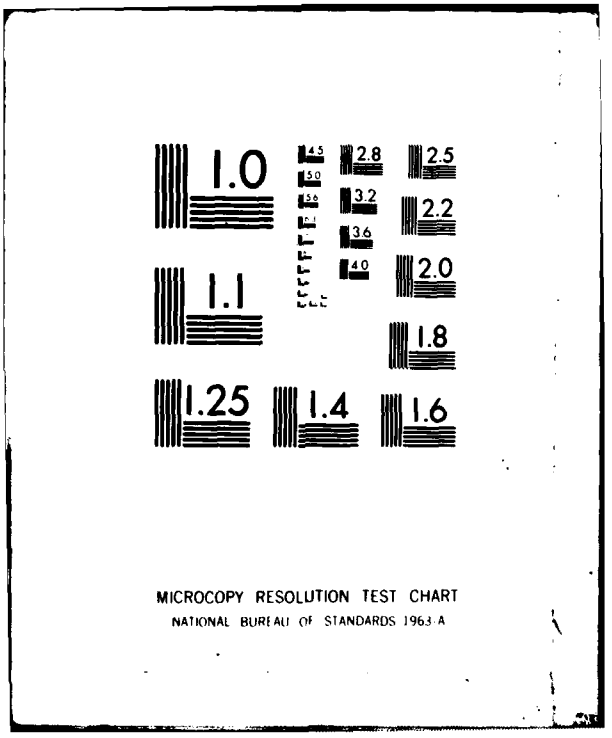
1.0
1.1
1.25
1.4
1.6
1.8
2.0
2.2
2.5
2.8
3.2
3.6
4.0
MICROCOPY RESOLUTION TEST CHART
NATIONAL BUREAU OF STANDARDS 1963-A

Figure (3-6) Peak 32 Desorption Spectra For Pure O_2 (A) And A 1.59% O_3 In O_2 Mixture (B).

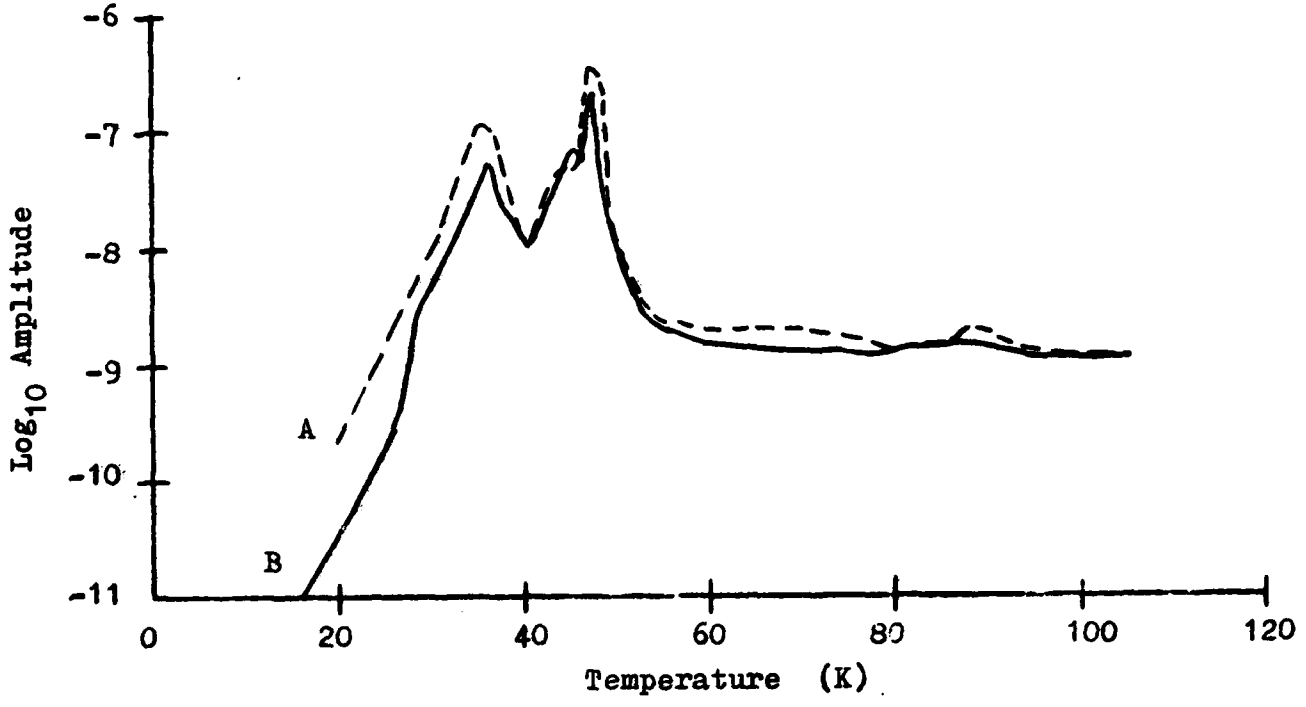

Figure (3-7) Ozone Regeneration Data.

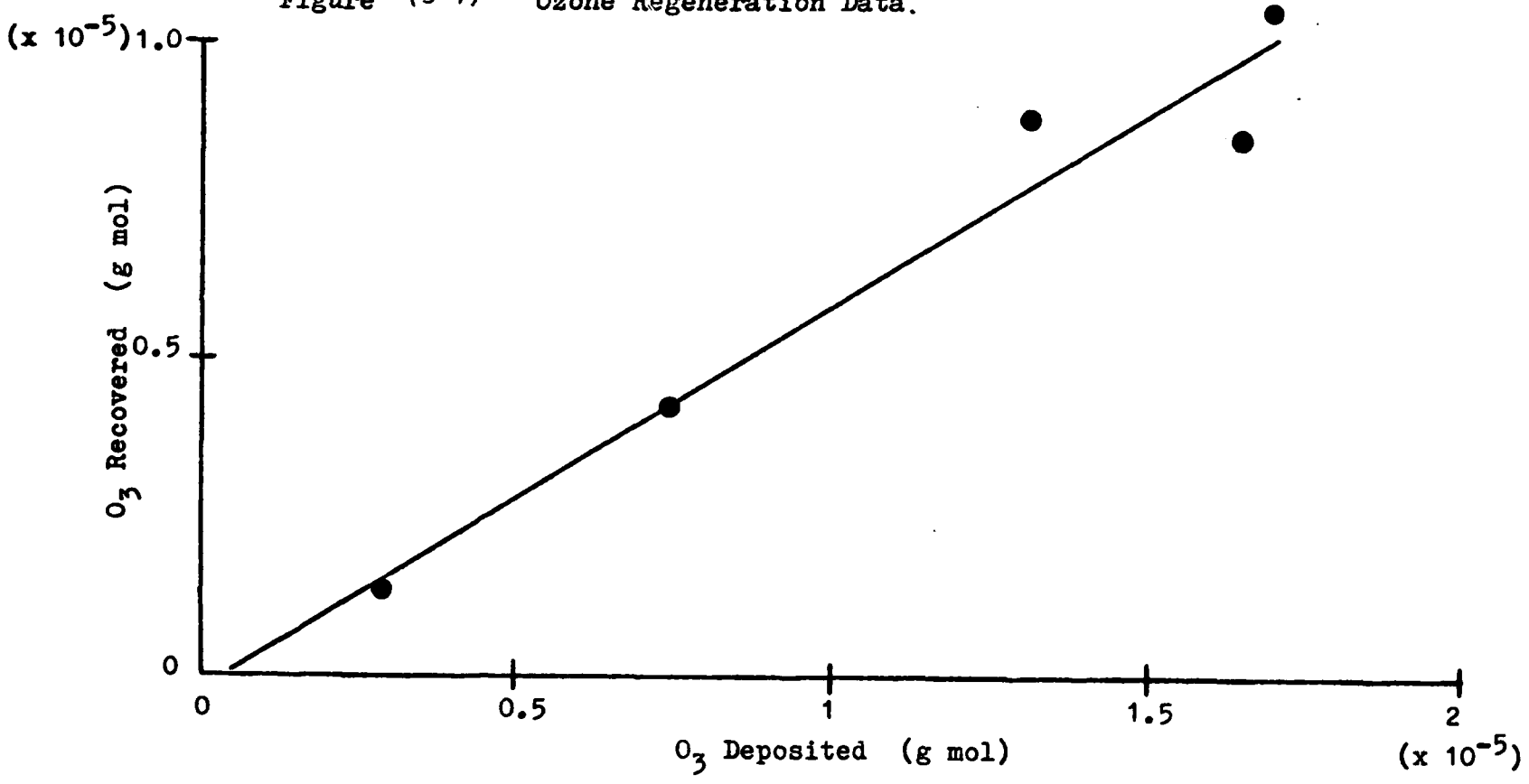

Figure (3-8) Ozone Conversion Versus Deposit Quantity.

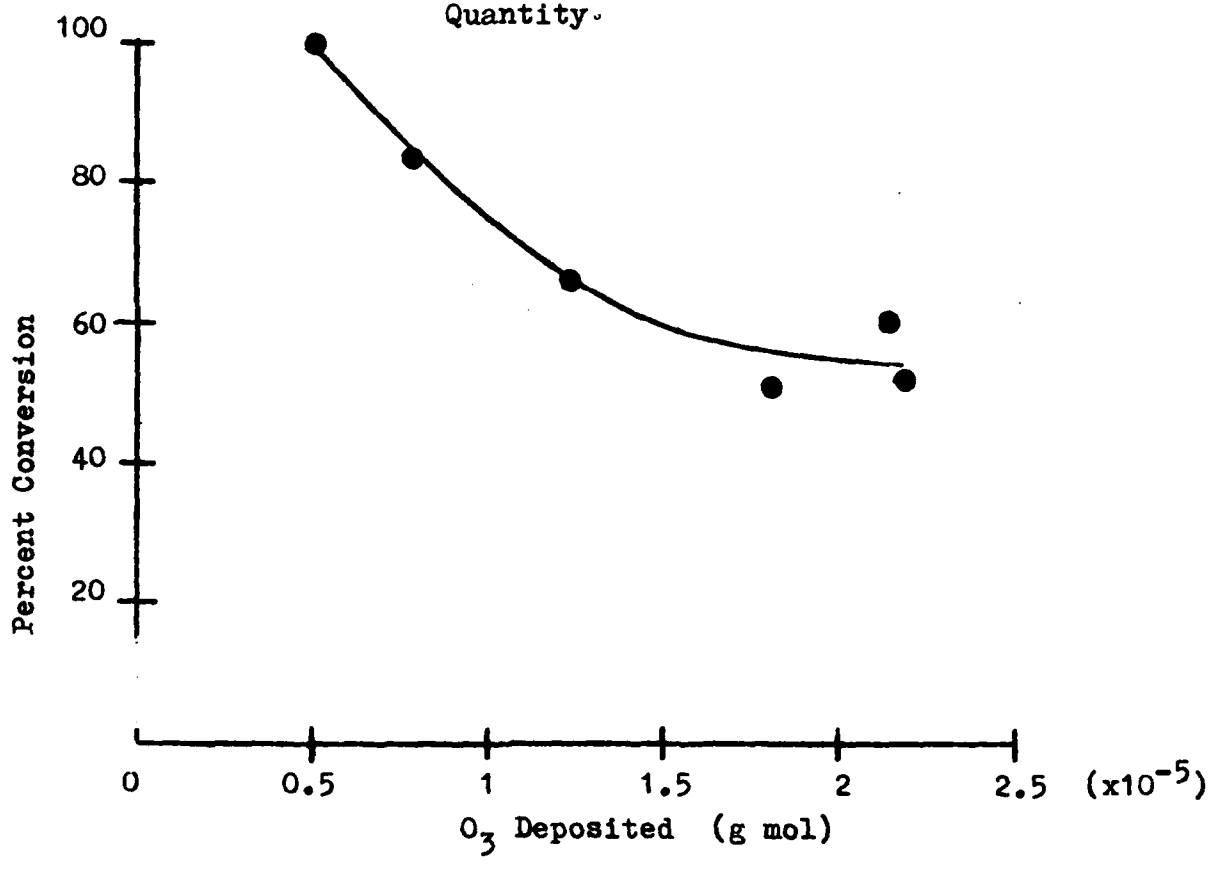

Figure (3-9) Ozone Regeneration Data.

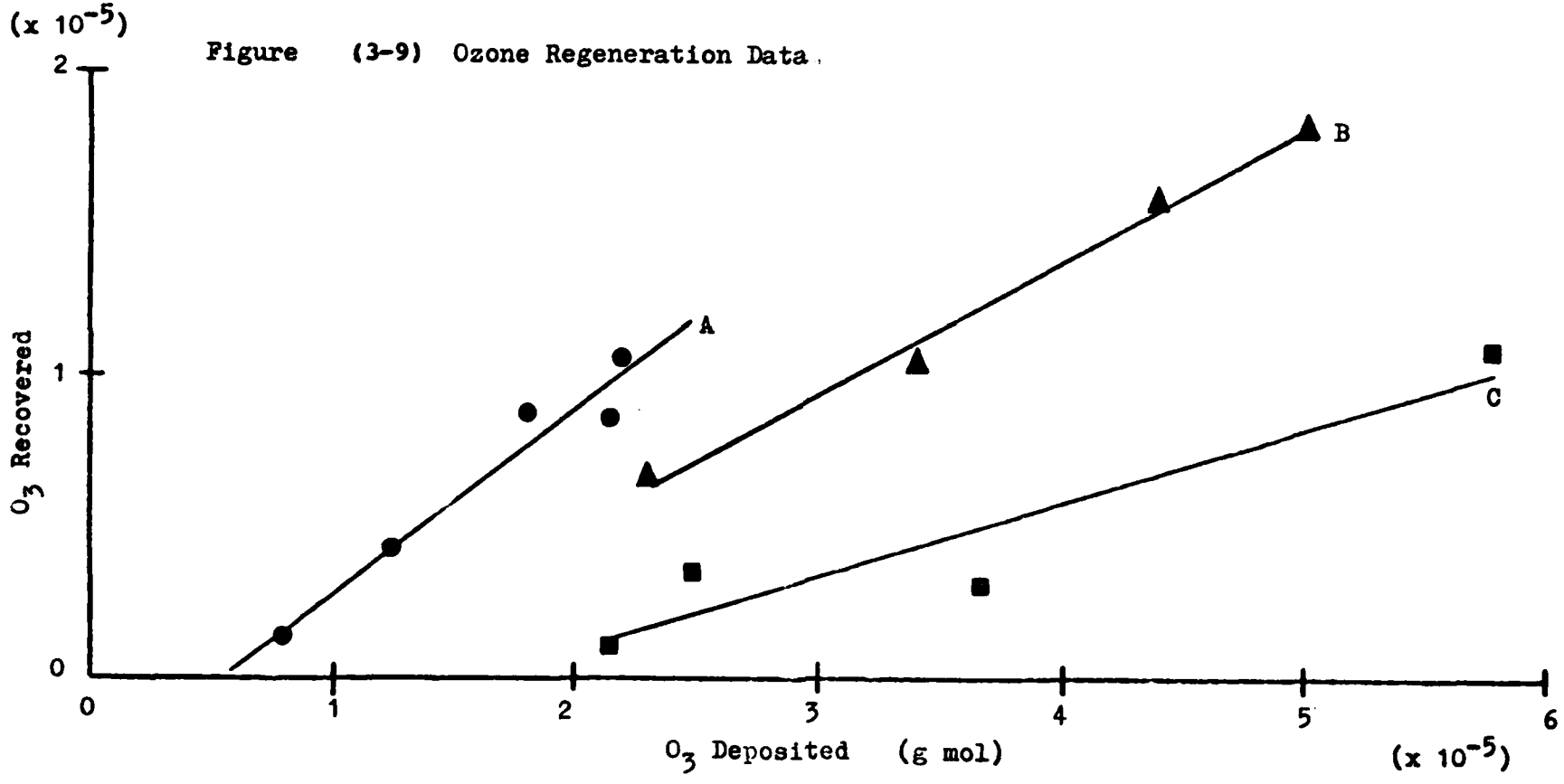

Figure (3-10). IR Spectrum of Condensed N_2O Sample Taken Soon After Deposition at a Sample Window Temperature of 18K (Vacuum Shroud Background Pressure of ∿ 1 mtorr).

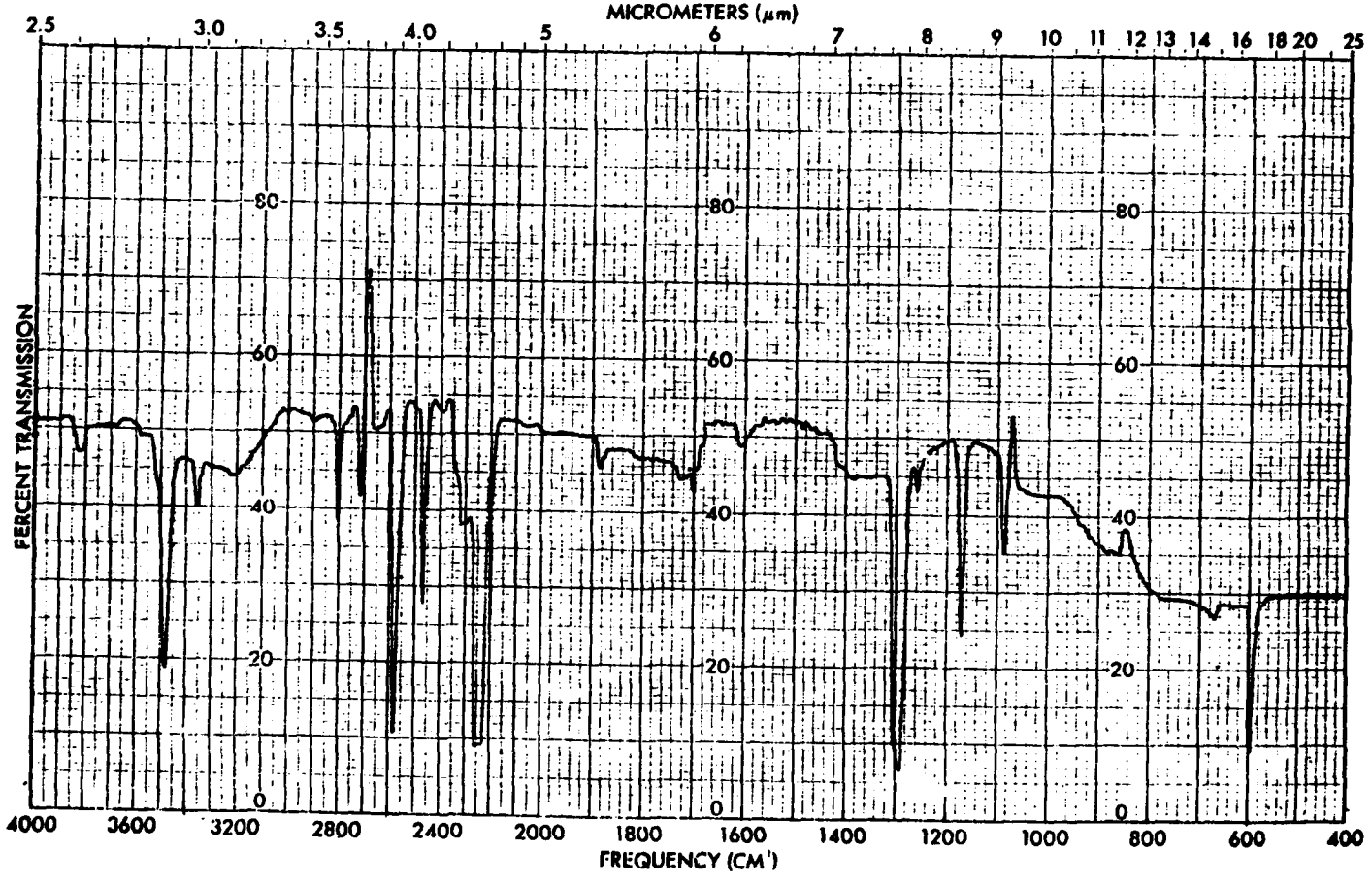
MICROMETERS (μm)
2.5
3.0
3.5
4.0
5
6
7
8
9
10
11
12
13
14
16
18
20
25
PERCENT TRANSMISSION
80
60
40
20
0
4000
3600
3200
2800
2400
2000
1800
1600
1400
1200
1000
800
600
400
FREQUENCY (CM⁻¹)

Figure (3-11). IR Spectrum of Condensed N_2O Sample Taken One Hour After Deposition at a Sample Window Temperature of 19K.

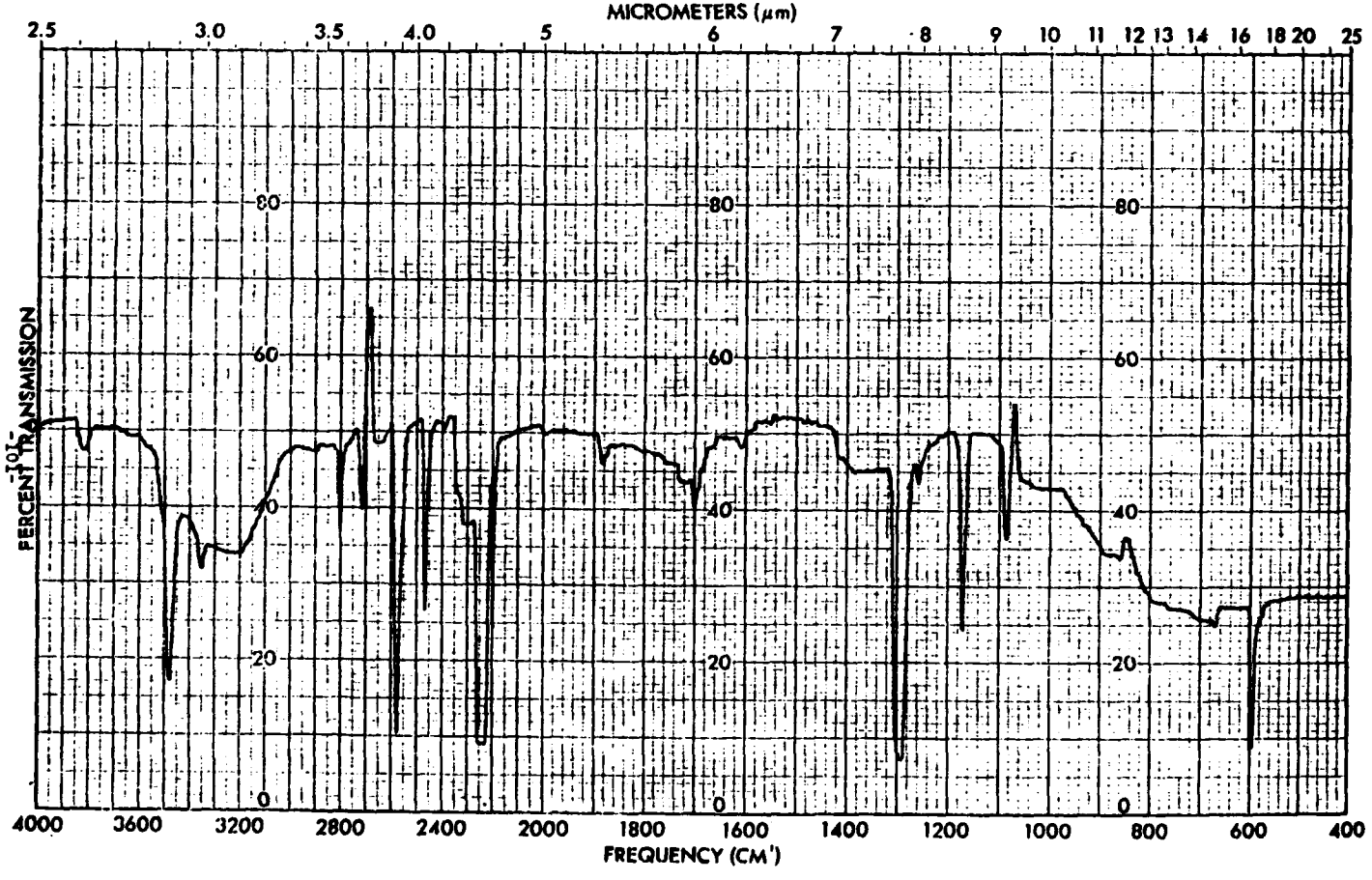
MICROMETERS (μm)
2.5
3.0
3.5
4.0
5
6
7
8
9
10
11
12
13
14
16
18
20
25
PERCENT TRANSMISSION
100
80
60
40
20
0
4000
3600
3200
2800
2400
2000
1800
1600
1400
1200
1000
800
600
400
FREQUENCY (CM')

Figure (3-12). Variation of Condensed N_2O Sample Spectrum with Temperature in the Vicinity of 3200 cm^{-1}.

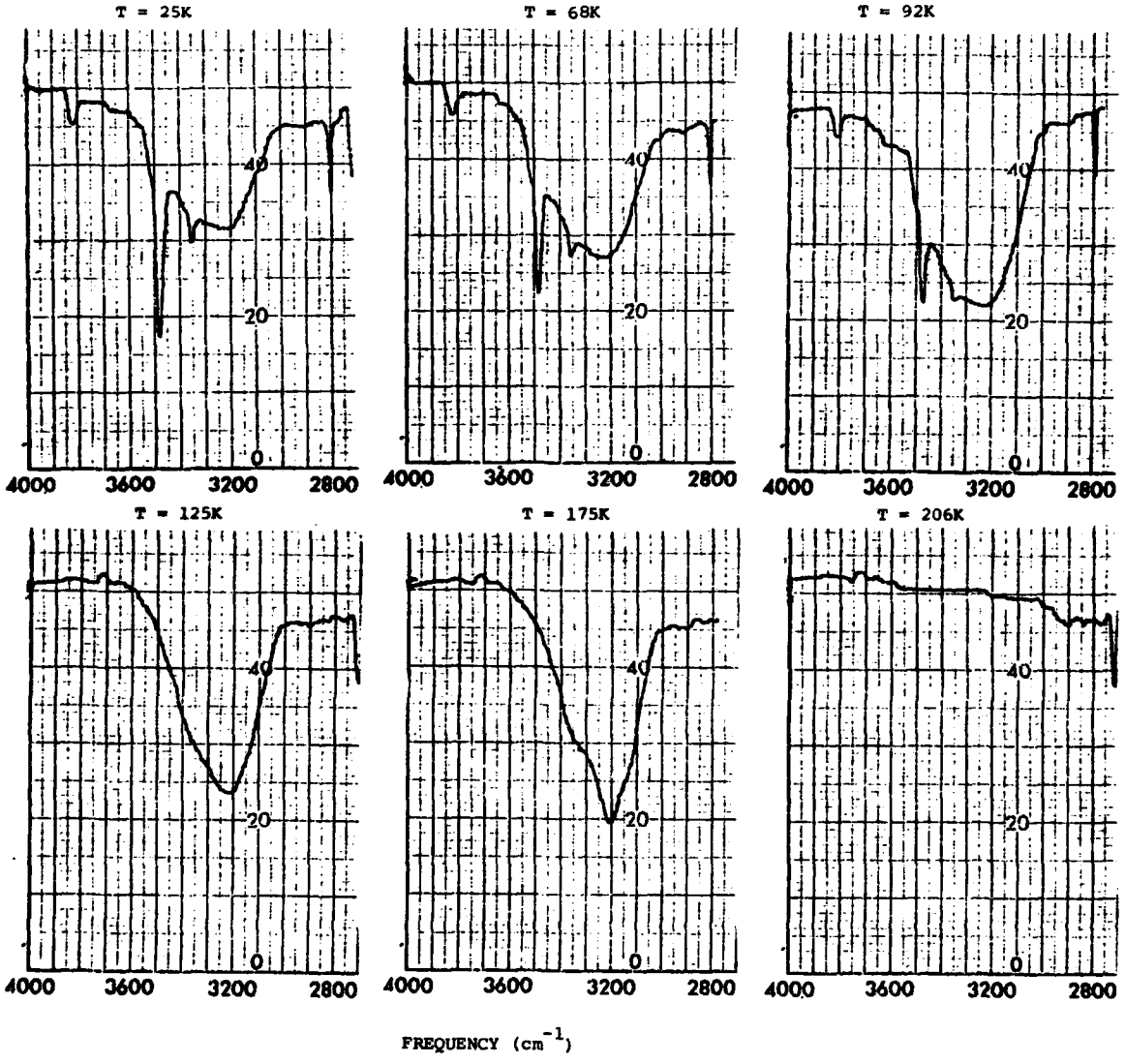
T = 25K
T = 68K
T = 92K
T = 125K
T = 175K
T = 206K
40
20
0
4000
3600
3200
2800
PERCENT TRANSMISSION
FREQUENCY (cm^{-1})

Figure (3-13). IR Spectrum of Sample Window at 17K With no N_2O Condensed Sample (Vacuum Shroud Background Pressure of ∿ 1 mtorr).

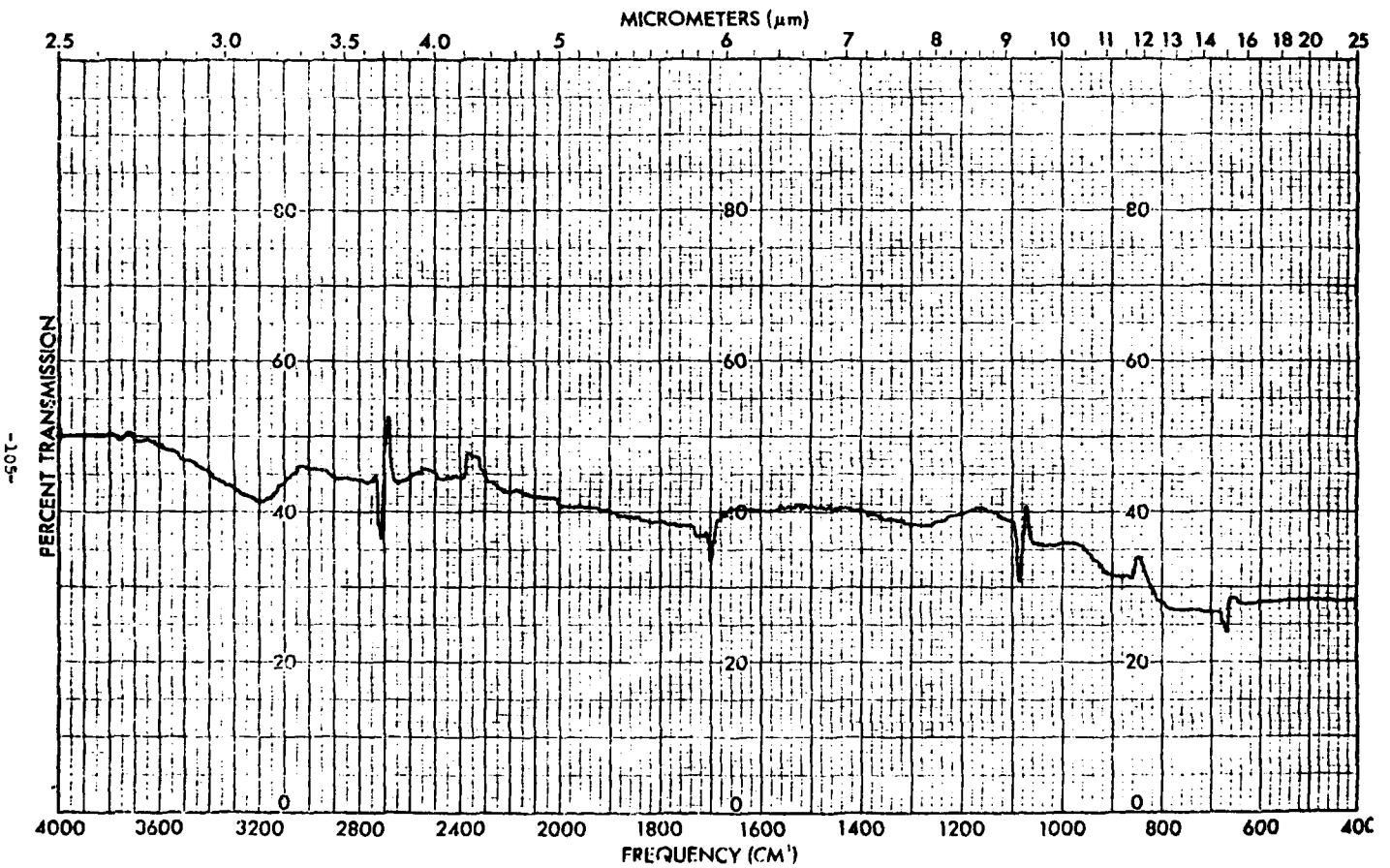
MICROMETERS (μm)
2.5
3.0
3.5
4.0
5
6
7
8
9
10
11
12
13
14
16
18
20
25
PERCENT TRANSMISSION
100
80
60
40
20
0
4000
3600
3200
2800
2400
2000
1800
1600
1400
1200
1000
800
600
400
FREQUENCY (CM⁻¹)

Figure (3-14). IR Spectra of Condensed CCl_2F_2 Sample at 20K (Vacuum Shroud Background Pressure at ∿ 1 mtorr): (A) Accuracy Mode, Blocked Reference Beam, Transmission set at 100%; (B) Accuracy Mode, Blocked Reference Beam, Transmission set at 80%; and (C) Resolution mode (Gain is 4 Times Less).

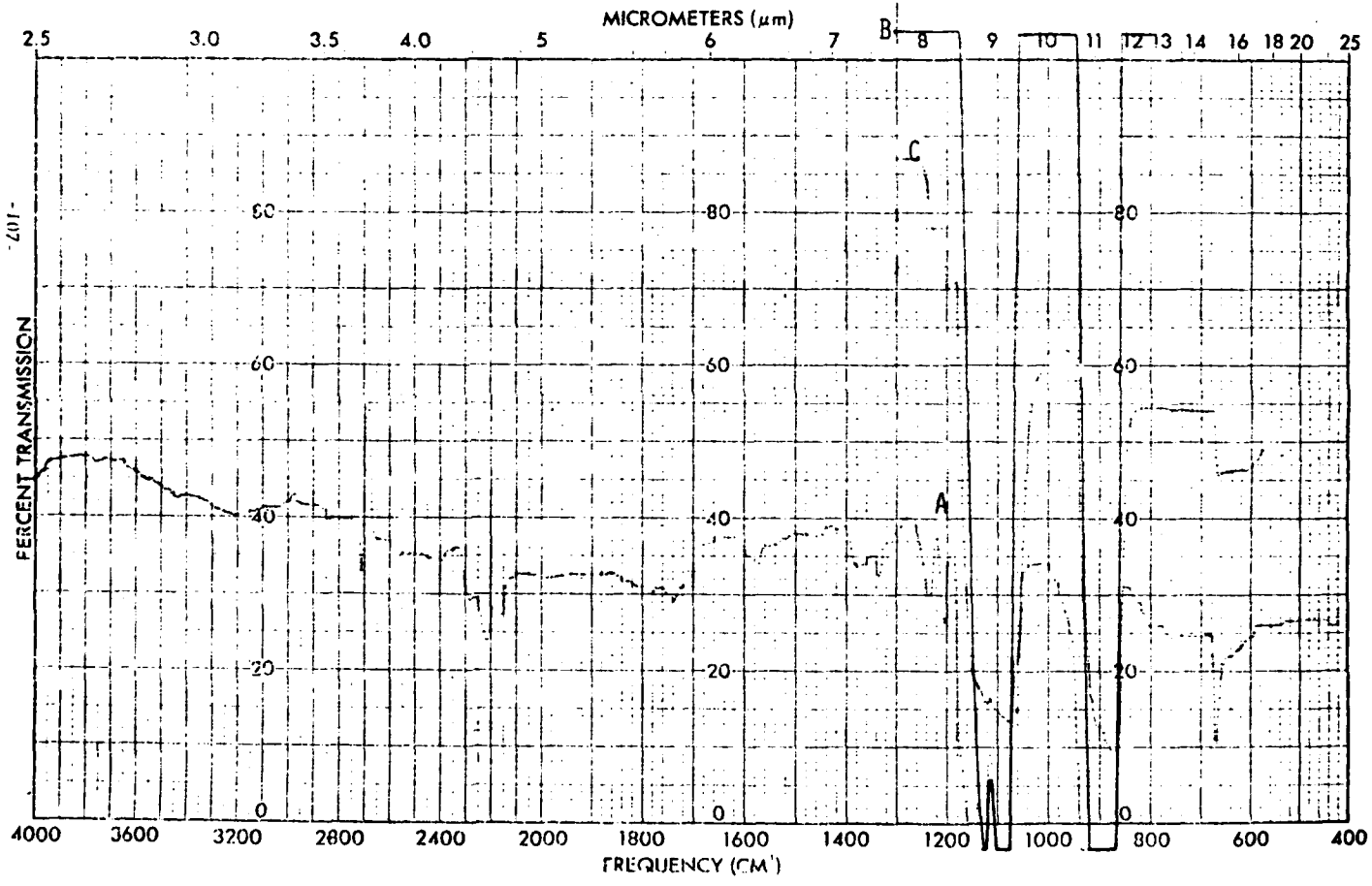
MICROMETERS (μm)
2.5
3.0
3.5
4.0
5
6
7
B
8
9
10
11
12
13
14
16
18
20
25
C
A
PERCENT TRANSMISSION
100
80
60
40
20
0
4000
3600
3200
2800
2400
2000
1800
1600
1400
1200
1000
800
600
400
FREQUENCY (CM⁻¹)

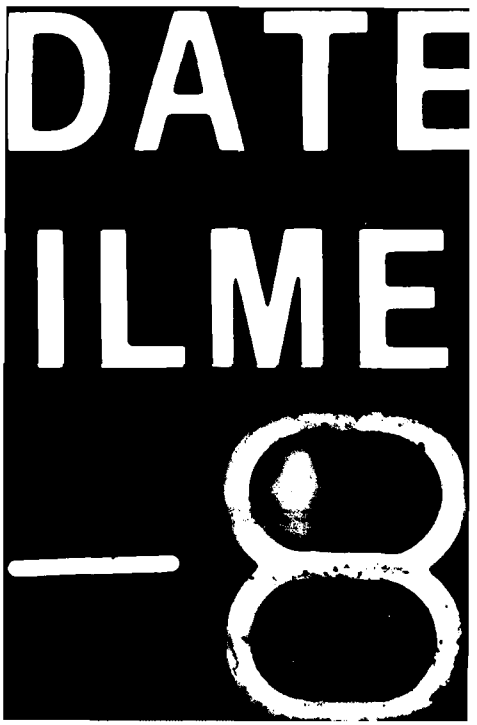
DATE
ILME
8